ACADÉMIE
DES SCIENCES
INSTITUT DE FRANCE

Comptes Rendus
Mécanique

Nagham Chibli, Martin Genet and Sébastien Imperiale

A class of optimal virtual fields for inverse problems in elasticity

Volume 354 (2026), p. 417-449

Online since: 4 May 2026

https://doi.org/10.5802/crmeca.361

The Comptes Rendus. Mécanique *are a member of the Mersenne Center for open scientific publishing*
www.centre-mersenne.org — e-ISSN : 1873-7234

ACADÉMIE DES SCIENCES
INSTITUT DE FRANCE

Comptes Rendus. Mécanique
2026, Vol. 354, p. 417-449
https://doi.org/10.5802/crmeca.361

Research article

A class of optimal virtual fields for inverse problems in elasticity

Nagham Chibli[a,b,c], **Martin Genet**[a] **and Sébastien Imperiale**[*,b,c]

[a] LMS, École Polytechnique, IPP – CNRS, France

[b] Inria, Inria-Saclay Île de France, France

[c] CMAP, École Polytechnique, IPP – CNRS, France

E-mail: sebastien.imperiale@inria.fr

Abstract. This work addresses the identification of nonhomogeneous constitutive parameters from full-field measurements in both linear and nonlinear elasticity, considering incompressible as well as compressible materials. The inverse identification procedure relies on the Virtual Fields Method (VFM), which is based on the principle of virtual work with specifically chosen virtual fields. We propose an optimal class of virtual fields, designed to optimize the reconstruction stability with respect to measurement noise. A series of numerical experiments illustrate the effectiveness of the proposed approach. The method exhibits moderate sensitivity to measurement noise and remains robust even when the boundary conditions are only partially known.

Keywords. Parameter identification, virtual fields method, elasticity, inverse problem.

Manuscript received 15 January 2026, revised 1 April 2026, accepted 2 April 2026, online since 4 May 2026.

1. Introduction

Inverse problems are widely encountered in applied sciences and engineering, where they serve notably to estimate unknown material parameters from indirect or incomplete observations. In this context, full-field measurement techniques have led to major advances in the identification of the mechanical behavior of solids [1–3].

In biomechanics and medical imaging, these approaches are particularly relevant for the study of soft biological tissues, whose mechanical properties can provide valuable diagnostic information [4,5]. Indeed, numerous studies over the past few decades have shown that these properties vary significantly with age, pathology, and physiological conditions [6,7]. However, these techniques are not limited to biomedical applications. They have also proven highly effective in solid mechanics, where they are employed to identify elastic properties of composite materials, characterize anisotropic behavior in wood, and analyze fracture mechanisms or damage evolution in heterogeneous structures [8,9].

This framework involves two coupled inverse problems. The first concerns imaging and image processing, which provides full-field measurements of displacement fields. The second uses these displacement measurements to reconstruct the underlying mechanical properties of the material.

* Corresponding author

For the first inverse problem, advances in imaging and computational methods, such as ultrasound [10,11], Magnetic Resonance Imaging (MRI) [12,13], and Optical Coherence Tomography (OCT) [14], followed by image processing techniques such as Digital Image Correlation (DIC) [15–17], have enabled the acquisition and extraction of high-resolution full-field displacement data.

For the second inverse problem, state-of-the-art techniques provide a variety of approaches to reconstruct mechanical properties from full-field data, which can generally be categorized into iterative and direct methods. Notable iterative methods include the Finite Element Model Updating (FEMU) approach [18–20], which minimizes the difference between experimental and simulated displacement, and the Constitutive Equation Gap Method (CEGM) [3,21–23], which identifies elastic parameters by minimizing the constitutive relation error. While effective and highly robust, these methods are computationally expensive.
On the other hand, direct inversion methods have been employed for identifying both homogeneous and heterogeneous elastic properties. The core idea is that elastic parameters can be explicitly expressed in terms of measured displacement or strain fields, thus providing a direct solution to the inverse problem. These methods are computationally efficient and well-suited for the rapid estimation of material properties. Examples include the Equilibrium Gap Method (EGM) [20,24], which minimizes the residuals in the equilibrium equations, and the Reciprocity Gap Method (RGM) [25,26], which leverages reciprocal work theorems to solve inverse problems in elasticity. Other approaches treat the problem as a partial differential equation (PDE) in the material parameters, where the measurements act as coefficients or source terms in this equation [27–29]. While these methods allow for the reconstruction of spatially distributed parameters, existing approaches generally exhibit a strong sensitivity to measurement noise. To address the inherent ill-posedness of such inverse problems and to ensure stability, particularly when reconstructing nonhomogeneous distributions of mechanical properties, regularization terms are typically introduced to prevent overfitting [30,31]. However, even with regularization, these methods often remain sensitive to measurement noise and depend on high-resolution, full-field displacement data. To mitigate these issues and improve robustness, several strategies have been proposed, such as the reconditioned EGM [32] and displacement filtering techniques [20].

Another widely used approach is the Virtual Fields Method (VFM), which was proposed several decades ago [33] and has since been applied to a wide range of problems [34,35]. The method relies on the principle of virtual work combined with a carefully chosen set of virtual fields, leading to a system of equations for the identification of material parameters. A central aspect of the VFM is therefore the choice of these virtual fields, as it strongly affects the accuracy and robustness of the reconstruction.

Early implementations of the VFM mainly relied on manually defined virtual fields, designed to satisfy kinematic admissibility and to simplify the extraction of constitutive parameters from full-field measurements. Such fields typically included piecewise continuous fields defined over subdomains [36] or low-order analytical functions, such as polynomials or simple basis functions [34,37,38]. Other analytical choices, including plane-wave virtual fields, have been introduced to improve sensitivity properties [20]. More recently, several works have addressed the inherent ill-posedness of the VFM, especially when reconstructing nonhomogeneous elastic property distributions, by introducing regularization strategies within the VFM framework [39]. In addition, solution-driven virtual fields, constructed from an intermediate configuration obtained by solving the forward problem with parameters close to the deformed state, have been proposed to address the reconstruction of the material distribution without the partition information [40]. Several methods have proposed classes of virtual fields in order to address the sensitivity to noise, both in linear and nonlinear elasticity, [37,41–43]. In this work, we propose an alternative strategy for the construction of virtual fields, designed to ensure stable and accurate parameter reconstruction by satisfying specific stability criteria. This method is formulated within a mathemat-

ical framework at the continuous level, which makes it possible to distinguish between noise-induced and discretization biases, and could be extended to the nonlinear case. We consider nonhomogeneous elastic solids, both compressible and incompressible, in which the nonhomogeneous regions are assumed to be known a priori. The paper is organized as follows. In Section 2, we first present the principle of virtual fields in the context of linear elasticity for compressible materials. We then introduce the definition of the proposed optimal virtual fields, describe their computation, and provide a stability analysis. In Section 3, the approach is extended to nearly incompressible and incompressible materials, as well as to a finite strain setting. In Section 4, we present two numerical applications to illustrate and validate the method. The first concerns the reconstruction of the shear modulus in compressible linear elasticity, while the second addresses the reconstruction of elastic parameters (Young's modulus, shear modulus, and Poisson's ratio) in compressible transversely isotropic linear elasticity.

2. Proposed method for the linear compressible elasticity

In this section, we introduce the proposed virtual fields method in the setting of linear compressible elasticity.

2.1. *Problem setting: the virtual fields method*

In the context of linear elasticity, we consider a solid body of arbitrary shape occupying a bounded domain $\Omega \subset \mathbb{R}^d$, with $d = 2$ or 3. A prescribed displacement is imposed on a portion of the boundary denoted by Γ_D, while a prescribed traction is applied on the complementary part Γ_N (see Figure 1). The displacement field is denoted by $\mathbf{u}$, and the associated strain tensor is given by

$$\boldsymbol{\varepsilon}(\mathbf{u}) := \frac{1}{2}(\nabla \mathbf{u} + \nabla \mathbf{u}^T).$$

The Virtual Fields Method (VFM) is based on the principle of virtual work, which corresponds to the weak form of the equilibrium equations. For an elastic body subjected to body forces, the virtual work principle can be expressed as

$$\int_\Omega \boldsymbol{\sigma}(\mathbf{u}) : \boldsymbol{\varepsilon}(\mathbf{v}) \, \mathrm{d}\Omega = \int_{\Gamma_N} \mathbf{t} \cdot \mathbf{v} \, \mathrm{d}\Gamma + \int_\Omega \mathbf{f} \cdot \mathbf{v} \, \mathrm{d}\Omega. \tag{1}$$

Here, $\boldsymbol{\sigma}(\mathbf{u})$ denotes the stress tensor associated with the displacement field $\mathbf{u}$ through the constitutive relation, $\boldsymbol{\varepsilon}(\mathbf{v})$ the virtual strain tensor associated with the virtual displacement field $\mathbf{v}$ and $\mathbf{t}$ the traction vector prescribed on the Neumann boundary Γ_N.

Equation (1) must hold for any kinematically admissible virtual field $\mathbf{v}$, that is, any $\mathbf{v} \in H^1(\Omega)^d$ vanishing on the Dirichlet boundary Γ_D, where displacements are prescribed (see Figure 1). We

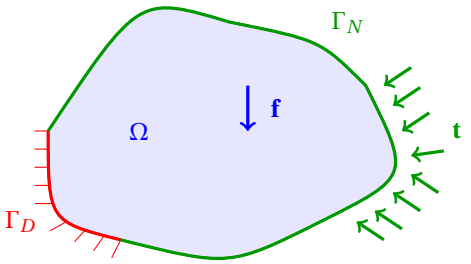

Figure 1. A solid of arbitrary geometry subjected to a prescribed displacement on Γ_D and a prescribed traction on Γ_N.The green arrows indicate the nonzero traction.

denote by $\mathbf{V} \coloneqq H^1(\Omega)^d$ the space of admissible displacement fields, equipped with the scalar product $(\cdot,\cdot)_{\mathbf{V}}$, and by

$$\mathbf{V}_0 \coloneqq H^1_{0,D}(\Omega)^d \subset \mathbf{V},$$

the subspace of kinematically admissible virtual fields, namely

$$\mathbf{V}_0 = \left\{\mathbf{v} \in H^1(\Omega)^d \;\middle|\; \mathbf{v} = \mathbf{0} \text{ on } \Gamma_D\right\}.$$

In this linear context, the stress tensor $\boldsymbol{\sigma}$ is related to the strain tensor $\boldsymbol{\varepsilon}$ through the constitutive relation $\boldsymbol{\sigma} = \mathbb{C}(\mathbf{x}) : \boldsymbol{\varepsilon}$, where $\mathbb{C}(\mathbf{x})$ denotes the spatially dependent fourth-order elasticity tensor.

The virtual work principle (1) can then be recast into a general variational form as

$$a_{\mathbb{C}}(\mathbf{u},\mathbf{v}) = \ell(\mathbf{v}), \quad \forall\, \mathbf{v} \in \mathbf{V}_0, \tag{2}$$

where $a_{\mathbb{C}} : \mathbf{V} \times \mathbf{V}_0 \to \mathbb{R}$ is the continuous bilinear form defined by

$$a_{\mathbb{C}}(\mathbf{u},\mathbf{v}) = \int_\Omega \mathbb{C} : \boldsymbol{\varepsilon}(\mathbf{u}) : \boldsymbol{\varepsilon}(\mathbf{v})\, \mathrm{d}\Omega, \tag{3}$$

with an associated continuity constant C_a satisfying

$$\left|a_{\mathbb{C}}(\mathbf{u},\mathbf{v})\right| \leq C_a \|\mathbf{u}\|_{\mathbf{V}} \|\mathbf{v}\|_{\mathbf{V}}. \tag{4}$$

The linear continuous functional $\ell : \mathbf{V}_0 \to \mathbb{R}$ is defined by

$$\ell(\mathbf{v}) = \int_{\Gamma_N} \mathbf{t}\cdot\mathbf{v}\,\mathrm{d}\Gamma + \int_\Omega \mathbf{f}\cdot\mathbf{v}\,\mathrm{d}\Omega. \tag{5}$$

Due to the linear dependence of the bilinear form $a_{\mathbb{C}}$ on the elasticity tensor $\mathbb{C}$, and assuming that $\mathbb{C}$ itself depends linearly on a set of parameters, we can write

$$a_{\mathbb{C}}(\mathbf{u},\mathbf{v}) = \sum_{k=1}^{m} a_k(\theta_k,\mathbf{u},\mathbf{v}),$$

where $\{\theta_k\}_{k=1}^m$ denotes the set of elastic parameters (e.g., the components of the elasticity tensor $\mathbb{C}$). Each parameter θ_k belongs to a Banach space X_k (in this work, these spaces are considered to be finite-dimensional), and for each $1 \leq k \leq m$, $a_k(\cdot,\cdot,\cdot)$ is a trilinear form on $X_k \times \mathbf{V} \times \mathbf{V}_0$ representing the contribution of the parameter θ_k to the internal virtual work.

2.2. *Discretization of the parameter space*

In this section, we aim to identify the set of parameters $\{\theta_k\}_{k=1}^m$, either in a nonhomogeneous solid (as illustrated in Figure 2), where the parameters are assumed to be piecewise constant over subregions known a priori, or, more generally, belonging to a finite-dimensional function space spanned by basis functions, i.e., each $\theta_k \in X_k$ with $X_k = \operatorname{span}\{\phi_{1,k},\ldots,\phi_{n,k}\} \subset L^\infty(\Omega)$, where, without loss of generality, we assume that all spaces X_k have the same dimension n. In both cases, the goal is to determine, for each $1 \leq k \leq m$, the coefficients $\{\alpha_{j,k}\}_{1\leq j\leq n}$ such that

$$\theta_k(\mathbf{x}) = \sum_{j=1}^{n} \alpha_{j,k}\,\phi_{j,k}(\mathbf{x}). \tag{6}$$

Equation (2) can then be written as

$$\sum_{k=1}^{m}\sum_{j=1}^{n} \alpha_{j,k}\, a_k(\phi_{j,k},\mathbf{u},\mathbf{v}) = \ell(\mathbf{v}). \tag{7}$$

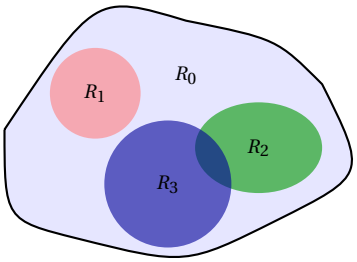

Figure 2. A nonhomogeneous domain where regions R_1, R_2, and R_3 represent inclusions with distinct material parameters, and R_0 denotes the background.

Single-parameter case. To simplify the development of our proposed method, we first consider the reconstruction of a single parameter

$$\theta(\mathbf{x}) = \sum_{j=1}^{n} \alpha_j \phi_j(\mathbf{x}), \tag{8}$$

where the functions $\{\phi_j\}_{j=1}^n$ are known. In this case, Eq. (7) reduces to

$$\sum_{j=1}^{n} \alpha_j \, a(\phi_j, \mathbf{u}, \mathbf{v}) = \ell(\mathbf{v}). \tag{9}$$

In practice, the load distribution $\mathbf{t}$ may be unknown and is generally much more difficult to measure than displacements. To address this difficulty, we restrict the choice of virtual fields to those that eliminate the traction term whenever the traction is unknown. More precisely, they are chosen in

$$\mathbf{K}_0 = \left\{ \mathbf{v} \in \mathbf{V}_0 \;\middle|\; \mathbf{T}\mathbf{v} = \mathbf{0} \text{ on } \Gamma_N \right\}, \tag{10}$$

where the matrix field $\mathbf{T} \in L^\infty(\Gamma_N)^{d\times d}$ is defined so that the virtual work associated with the traction $\mathbf{t}$ vanishes whenever $\mathbf{t}$ is unknown. Typical examples include $\mathbf{T} = \mathbf{0}$ when $\mathbf{t}$ is fully known, $\mathbf{T} = \mathbf{I}$ when all traction components are unknown, and, for instance, in the case $d = 2$, $\mathbf{T} = \mathbf{e} \otimes \mathbf{e}$ when $\mathbf{t}(\mathbf{x}) = t(\mathbf{x})\,\mathbf{e}(\mathbf{x})$, with t an unknown scalar and $\mathbf{e}$ a known vector field.

To avoid the system being under- or over-determined, we select exactly n kinematically admissible virtual fields $\{\mathbf{v}_i\}_{1\le i\le n} \subset \mathbf{K}_0$. Therefore, the problem (9) can be expressed in matrix form as

$$\boldsymbol{A}\boldsymbol{\alpha} = \boldsymbol{\lambda}, \tag{11}$$

where $\boldsymbol{A} \in \mathbb{R}^{n\times n}$ is defined by

$$\boldsymbol{A}_{ij} = a(\phi_j, \mathbf{u}, \mathbf{v}_i), \quad 1 \le i, j \le n,$$

$\boldsymbol{\lambda} \in \mathbb{R}^n$ is the right-hand side vector with entries

$$\boldsymbol{\lambda}_i = \ell(\mathbf{v}_i), \quad 1 \le i \le n,$$

and $\boldsymbol{\alpha} \in \mathbb{R}^n$ contains the unknown coefficients α_i.

Multi-parameter case. For the general case involving m parameters, we extend the approach by selecting $m \times n$ virtual fields to match the $m \times n$ unknowns, in order to avoid the system being over- or under-determined.

The kinematically admissible virtual fields $\{\mathbf{v}_i\}_{1\le i\le mn} \subset \mathbf{K}_0$ are chosen as before, and the global system is constructed as follows: the matrix $\boldsymbol{A} \in \mathbb{R}^{mn\times mn}$ is partitioned into m submatrices:

$$\boldsymbol{A} = \left[\boldsymbol{A}^{(1)} \; \cdots \; \boldsymbol{A}^{(m)} \right],$$

where $\boldsymbol{A}^{(k)} \in \mathbb{R}^{mn\times n}$ for $1 \le k \le m$ is given by

$$\boldsymbol{A}^{(k)}_{ij} = a_k(\phi_{j,k}, \mathbf{u}, \mathbf{v}_i), \quad 1 \le i \le mn,\ 1 \le j \le n.$$

More precisely, it takes the form

$$\boldsymbol{A}^{(k)} = \begin{pmatrix} a_k(\phi_{1,k}, \mathbf{u}, \mathbf{v}_1) & \cdots & a_k(\phi_{n,k}, \mathbf{u}, \mathbf{v}_1) \\ \vdots & \ddots & \vdots \\ a_k(\phi_{1,k}, \mathbf{u}, \mathbf{v}_{mn}) & \cdots & a_k(\phi_{n,k}, \mathbf{u}, \mathbf{v}_{mn}) \end{pmatrix}, \quad 1 \le k \le m.$$

The right-hand side $\boldsymbol{\lambda} \in \mathbb{R}^{mn}$ remains

$$\boldsymbol{\lambda}_i = \ell(\mathbf{v}_i), \quad 1 \le i \le mn.$$

The unknown vector $\boldsymbol{\alpha} \in \mathbb{R}^{mn}$ groups the coefficients for all parameters, namely,

$$\boldsymbol{\alpha} = \begin{pmatrix} \boldsymbol{\alpha}^{(1)} \\ \vdots \\ \boldsymbol{\alpha}^{(m)} \end{pmatrix}, \quad \text{where } (\boldsymbol{\alpha}^{(k)})_j = \alpha_{j,k},\ 1 \le k \le m,\ 1 \le j \le n.$$

The final system is compactly written as

$$\boldsymbol{A}\boldsymbol{\alpha} = \boldsymbol{\lambda}. \tag{12}$$

Insight into the stability analysis. Our problem enters the following general class of inverse problems. Let X and W be two normed vector spaces. For a given state variable $\mathbf{u} \in X$ and a sequence of virtual fields $\mathbf{v} = (\mathbf{v}_1, \dots, \mathbf{v}_N) \in W$, we define a matrix-valued mapping

$$\boldsymbol{A}\colon X \times W \longrightarrow \mathbb{R}^{N\times N},$$

and a vector-valued mapping

$$\boldsymbol{\lambda}\colon W \longrightarrow \mathbb{R}^{N}.$$

Here, for simplicity, we assume that $\boldsymbol{\lambda}$ is independent of $\mathbf{u}$. For a fixed sequence of virtual fields $\mathbf{v}$, the unknown vector $\boldsymbol{\alpha} \in \mathbb{R}^N$ is obtained by solving

$$\boldsymbol{A}(\mathbf{u}, \mathbf{v})\, \boldsymbol{\alpha} = \boldsymbol{\lambda}(\mathbf{v}). \tag{13}$$

We assume that both $\boldsymbol{A}$ and $\boldsymbol{\lambda}$ are linear with respect to $\mathbf{v}$ and, moreover, that the mapping $\boldsymbol{A}$ is Lipschitz continuous with respect to $\mathbf{u}$, i.e.

$$\left\| \boldsymbol{A}(\mathbf{u}, \mathbf{v}) - \boldsymbol{A}(\widetilde{\mathbf{u}}, \mathbf{v}) \right\|_2 \le C_A \|\mathbf{u} - \widetilde{\mathbf{u}}\|_X \|\mathbf{v}\|_W.$$

where $\|\cdot\|_2$ denotes the Euclidean norm for vectors and the associated induced matrix norm, and C_A is a positive constant. Let $\mathbf{u}^0$ denote the exact displacement field and $\mathbf{u}^\delta$ a perturbed measurement satisfying

$$\|\mathbf{u}^\delta - \mathbf{u}^0\|_X \le \delta,$$

where $\delta > 0$ represents the noise level. We define

$$\boldsymbol{A}^0 := \boldsymbol{A}(\mathbf{u}^0, \mathbf{v}) \qquad \text{and} \qquad \boldsymbol{A}^\delta := \boldsymbol{A}(\mathbf{u}^\delta, \mathbf{v}).$$

The corresponding solutions $\boldsymbol{\alpha}^0$ and $\boldsymbol{\alpha}^\delta$ satisfy

$$\boldsymbol{A}^0 \boldsymbol{\alpha}^0 = \boldsymbol{\lambda}, \qquad \boldsymbol{A}^\delta \boldsymbol{\alpha}^\delta = \boldsymbol{\lambda}. \tag{14}$$

Assuming that $\boldsymbol{A}^\delta$ is invertible, we obtain

$$\boldsymbol{\alpha}^0 - \boldsymbol{\alpha}^\delta = (\boldsymbol{A}^\delta)^{-1}(\boldsymbol{A}^\delta - \boldsymbol{A}^0)\boldsymbol{\alpha}^0.$$

Hence

$$\|\boldsymbol{\alpha}^0 - \boldsymbol{\alpha}^\delta\|_2 \le \left\|(\boldsymbol{A}^\delta)^{-1}\right\|_2 \|\boldsymbol{A}^\delta - \boldsymbol{A}^0\|_2 \|\boldsymbol{\alpha}^0\|_2.$$

Using the Lipschitz estimates above, we obtain

$$\frac{\|\boldsymbol{\alpha}^0 - \boldsymbol{\alpha}^\delta\|_2}{\|\boldsymbol{\alpha}^0\|_2} \leq \left(C_A \|\mathbf{u}^0\|_X\right)\left(\left\|(\boldsymbol{A}^\delta)^{-1}\right\|_2 \|\mathbf{v}\|_W\right) \frac{\|\mathbf{u}^\delta - \mathbf{u}^0\|_X}{\|\mathbf{u}^0\|_X}.$$

Therefore, if the virtual fields are chosen such that $\|\mathbf{v}\|_W = 1$ (indeed, due to the linearity of $\boldsymbol{A}$ and $\boldsymbol{\lambda}$, the virtual fields are chosen up to a multiplicative constant), then for a given measurement $\mathbf{u}^\delta$, the relative reconstruction error on $\boldsymbol{\alpha}$ can be minimized by minimizing $\left\|(\boldsymbol{A}^\delta)^{-1}\right\|_2 = \left\|\boldsymbol{A}(\mathbf{u}^\delta, \mathbf{v})^{-1}\right\|_2$ with respect to $\mathbf{v}$ on the unit sphere. In what follows, since the dependence of $\left\|(\boldsymbol{A}^\delta)^{-1}\right\|_2$ on $\mathbf{v}$ is intricate, the class of virtual fields we propose first makes the matrix $\boldsymbol{A}^\delta$ diagonal and then minimizes $\left\|(\boldsymbol{A}^\delta)^{-1}\right\|_2$ on the unit sphere. Note that this class of virtual fields depends on the measured displacement field. More detailed stability estimates will be established in the following sections.

2.3. *The single-parameter case*

2.3.1. *Definition and computation of optimal virtual fields*

In this section, we discuss the selection of virtual fields, which plays a crucial role in the accuracy of the reconstruction, as discussed in the previous section. To clearly illustrate the methodology, we restrict our discussion to the case of single-parameter reconstruction. The extension to multiple-parameter reconstruction follows the same principles and is presented in Section 2.4.

Therefore, we consider the problem of reconstructing the coefficients $\{\alpha_j\}_{j=1}^n$ defined in (8), which, according to the previous section, correspond to the unknowns of system (11), from the displacement field $\mathbf{u}$.

Single-coefficient reconstruction. We assume $n = 1$, that is, we aim to identify a single parameter θ, defined by a single coefficient α such that

$$\theta = \alpha\,\phi,$$

with ϕ known. We introduce this definition of virtual fields, which will be justified below in Remark 2 and, more generally, in Section 2.3.4.

Definition 1 (Single-parameter/single-coefficient case). *We define the virtual field* $\mathbf{v}_1$ *as the solution to the following maximization problem:*

$$\mathbf{v}_1 = \underset{\mathbf{v}\in\mathbf{K}_0,\ \|\mathbf{v}\|_{\mathbf{V}_0}\leq 1}{\arg\max} \quad a(\phi, \mathbf{u}, \mathbf{v}).$$

To compute $\mathbf{v}_1$, the results presented in the following paragraph apply. In particular, we show that $\mathbf{v}_1$ can be obtained by solving a linear variational problem.

Under the hypothesis that $a(\phi, \mathbf{u}, \mathbf{v}_1)$ is nonzero, the coefficient α to be reconstructed is then given by

$$\alpha = \frac{\ell(\mathbf{v}_1)}{a(\phi, \mathbf{u}, \mathbf{v}_1)}. \tag{15}$$

Remark 2. Here, we can justify this choice by providing some insight into the stability analysis with respect to noise. Indeed, if $\mathbf{u}^\delta$ is the noisy data corresponding to the noiseless data $\mathbf{u}^0$, solution to

$$\alpha^0\, a(\phi, \mathbf{u}^0, \mathbf{v}) = \ell(\mathbf{v}) \quad \forall\, \mathbf{v} \in \mathbf{V}_0, \tag{16}$$

and if we reconstruct the parameter α^δ by

$$\alpha^\delta = \frac{\ell^\delta(\mathbf{v}_1^\delta)}{a(\phi, \mathbf{u}^\delta, \mathbf{v}_1^\delta)},$$

with $\mathbf{v}_1^\delta$ defined as in Definition 1 using $\mathbf{u} = \mathbf{u}^\delta$, and ℓ^δ the counterpart of ℓ with noisy data, then by applying (16) with $\mathbf{v} = \mathbf{v}_1^\delta$, we obtain

$$\alpha^\delta a(\phi, \mathbf{u}^\delta, \mathbf{v}_1^\delta) - \alpha^0 a(\phi, \mathbf{u}^0, \mathbf{v}_1^\delta) = \ell^\delta(\mathbf{v}_1^\delta) - \ell(\mathbf{v}_1^\delta).$$

Hence, it follows that

$$|\alpha^0 - \alpha^\delta| \leq \frac{1}{\left|a(\phi, \mathbf{u}^\delta, \mathbf{v}_1^\delta)\right|}\left(\|\ell - \ell^\delta\|_{\mathbf{V}'} + C_a \|\mathbf{u}^\delta - \mathbf{u}^0\|_{\mathbf{V}}\right),$$

where C_a is defined in (4). Here, $\|\cdot\|_{\mathbf{V}'}$ denotes the dual norm on $\mathbf{V}'$, the space of continuous linear forms on V, defined by

$$\|\ell\|_{\mathbf{V}'} = \sup_{\mathbf{v}\in\mathbf{V},\ \mathbf{v}\neq 0} \frac{\left|\ell(\mathbf{v})\right|}{\|\mathbf{v}\|_{\mathbf{V}}}.$$

The idea is therefore to minimize

$$\frac{1}{\left|a(\phi, \mathbf{u}^\delta, \mathbf{v}_1^\delta)\right|},$$

and this choice will be extended to the case of multiple parameters and multiple coefficients.

In the following, we address the case of multiple coefficient reconstruction. The objective is to develop a method for computing the virtual fields and the reconstructed parameters, similar to the approach used in the single-coefficient case.

Multiple-coefficient reconstruction. When $n \geq 2$, we choose the virtual fields such that the matrix $\boldsymbol{A}$ is diagonal. More precisely, each virtual field $\mathbf{v}_i$ is selected in the subspace

$$\mathbf{H}_i := \left\{\mathbf{v} \in \mathbf{K}_0 \;\middle|\; a(\phi_j, \mathbf{u}, \mathbf{v}) = 0 \text{ for all } j \neq i\right\}.$$

This construction ensures the independent recoverability of each coefficient α_j, $1 \leq j \leq n$, from the system. We note that $\mathbf{H}_i$ is a closed vector subspace of $\mathbf{V}$, and hence a Hilbert space, endowed with the same inner product as $\mathbf{V}$.

Definition 3 (Single-parameter/multi-coefficient case). *We define the virtual fields* $\{\mathbf{v}_i\}_i$ *by*

$$\mathbf{v}_i = \operatorname*{arg\,max}_{\mathbf{v}\in\mathbf{H}_i,\ \|\mathbf{v}\|_{\mathbf{V}_0}\leq 1} f_i(\mathbf{v}), \tag{17}$$

where the continuous linear form f_i *is defined as*

$$\begin{aligned} f_i : \mathbf{V}_0 &\longrightarrow \mathbb{R}, \\ \mathbf{v} &\longmapsto a(\phi_i, \mathbf{u}, \mathbf{v}). \end{aligned} \tag{18}$$

We now address the question of computing $\mathbf{v}_i$.

Theorem 4. *The problem* (17) *admits at least one solution.*

Proof. We aim to show that the maximum of f_i over the closed unit ball of $\mathbf{H}_i$ defined by

$$B = \left\{\mathbf{w} \in \mathbf{H}_i \;\middle|\; \|\mathbf{w}\|_{\mathbf{V}_0} \leq 1\right\}. \tag{19}$$

is attained.

The functional f_i is linear and continuous on $\mathbf{H}_i$, and since $\mathbf{H}_i$ is a Hilbert space, by the Riesz representation theorem, there exists $\mathbf{h}_i \in \mathbf{H}_i$ such that

$$f_i(\mathbf{v}) = (\mathbf{h}_i, \mathbf{v})_{\mathbf{V}_0}, \quad \forall\ \mathbf{v} \in \mathbf{H}_i.$$

By the Cauchy–Schwarz inequality, we have

$$\forall\ \mathbf{v} \in B, \quad f_i(\mathbf{v}) = (\mathbf{h}_i, \mathbf{v})_{\mathbf{V}_0} \leq \|\mathbf{h}_i\|_{\mathbf{V}_0}\|\mathbf{v}\|_{\mathbf{V}_0} \leq \|\mathbf{h}_i\|_{\mathbf{V}_0},$$

hence f_i is bounded from above by $\|\mathbf{h}_i\|_{\mathbf{V}_0}$ on B. Therefore, there exists a maximizing sequence $\mathbf{v}_n \in B$ such that

$$f_i(\mathbf{v}_n) \longrightarrow \sup_{\mathbf{v}\in B} f_i(\mathbf{v}), \quad \text{as } n \to \infty.$$

Since $\mathbf{H}_i$ is a Hilbert space, it is reflexive, and hence the set B is weakly compact. Consequently, every sequence in B admits a weakly convergent subsequence. As $\mathbf{v}_n \in B$, there exists a subsequence, still denoted $\mathbf{v}_n$, that converges weakly to some $\mathbf{v}^* \in B$, i.e., $\mathbf{v}_n \rightharpoonup \mathbf{v}^*$ in $\mathbf{H}_i$ as $n \to \infty$. By the weak continuity of f_i, we have

$$f_i(\mathbf{v}_n) \longrightarrow f_i(\mathbf{v}^*) = (\mathbf{h}_i, \mathbf{v}^*)_{\mathbf{V}_0}, \quad \text{as } n \to \infty.$$

Therefore, the supremum is attained at $\mathbf{v}^*$, which concludes the proof. □

Theorem 5. *A solution to* (17) *is given by*

$$\mathbf{v}_i := \frac{\mathbf{h}_i}{\|\mathbf{h}_i\|_{\mathbf{V}_0}}, \tag{20}$$

where $\mathbf{h}_i$ *is the Riesz representative of the continuous linear functional* f_i *on* $\mathbf{H}_i$.

Proof. On the set B defined in (19), we have

$$f_i(\mathbf{v}) = (\mathbf{h}_i, \mathbf{v})_{\mathbf{V}_0} \le \|\mathbf{h}_i\|_{\mathbf{V}_0} \|\mathbf{v}\|_{\mathbf{V}_0} \le \|\mathbf{h}_i\|_{\mathbf{V}_0}.$$

Therefore,

$$\sup_{\substack{\mathbf{v}\in\mathbf{H}_i \\ \|\mathbf{v}\|_{\mathbf{V}_0}=1}} f_i(\mathbf{v}) \le \max_{\substack{\mathbf{v}\in\mathbf{H}_i \\ \|\mathbf{v}\|_{\mathbf{V}_0}\le 1}} f_i(\mathbf{v}) \le \|\mathbf{h}_i\|_{\mathbf{V}_0}. \tag{21}$$

Moreover, by choosing $\mathbf{v}_i = \frac{\mathbf{h}_i}{\|\mathbf{h}_i\|_{\mathbf{V}_0}}$, we get

$$\|\mathbf{h}_i\|_{\mathbf{V}_0} = (\mathbf{h}_i, \mathbf{v}_i)_{\mathbf{V}_0} \le \sup_{\substack{\mathbf{v}\in\mathbf{V} \\ \|\mathbf{v}\|_{\mathbf{V}_0}=1}} f_i(\mathbf{v}). \tag{22}$$

Combining (21) and (22), we obtain

$$f_i(\mathbf{v}_i) = \sup_{\substack{\mathbf{v}\in\mathbf{H}_i \\ \|\mathbf{v}\|_{\mathbf{V}_0}=1}} f_i(\mathbf{v}) = \max_{\substack{\mathbf{v}\in\mathbf{H}_i \\ \|\mathbf{v}\|_{\mathbf{V}_0}=1}} f_i(\mathbf{v}),$$

which allows us to conclude. □

As a consequence of this theorem, the proposed virtual fields satisfy, in practice, the following formulation:

$$\text{for } 1 \le i \le n, \quad \mathbf{v}_i = \frac{\mathbf{h}_i}{\|\mathbf{h}_i\|_{\mathbf{V}_0}}, \quad \text{with} \quad (\mathbf{h}_i, \mathbf{w})_{\mathbf{V}_0} = f_i(\mathbf{w}), \quad \forall\ \mathbf{w} \in \mathbf{H}_i.$$

In practice, to compute $\mathbf{h}_i$, we first determine $\mathbf{w}_i$, the Riesz representative of the functional f_i on the Hilbert space $\mathbf{V}_0$, satisfying

$$(\mathbf{w}_i, \mathbf{v})_{\mathbf{V}_0} = f_i(\mathbf{v}) \quad \forall\ \mathbf{v} \in \mathbf{V}_0,$$

then, we project it onto $\mathbf{H}_i$. This two-step procedure is justified by the following theorem.

Theorem 6. *Let* P_i *denote the orthogonal projection from* $\mathbf{V}_0$ *onto the closed subspace* $\mathbf{H}_i \subset \mathbf{V}_0$. *Then* $\mathbf{h}_i \in \mathbf{H}_i$ *satisfies*

$$\mathbf{h}_i = P_i \mathbf{w}_i.$$

Proof. The orthogonal projection $P_i : \mathbf{V}_0 \to \mathbf{H}_i$ is defined by the property

$$\big((I - P_i)\mathbf{v}, \mathbf{w}\big)_{\mathbf{V}_0} = 0, \quad \forall\, \mathbf{w} \in \mathbf{H}_i, \quad \forall\, \mathbf{v} \in \mathbf{V}_0.$$

In particular, for $\mathbf{w}_i \in \mathbf{V}_0$, we have for all $\mathbf{w} \in \mathbf{H}_i \subset \mathbf{V}_0$,

$$(P_i\mathbf{w}_i, \mathbf{w})_{\mathbf{V}_0} = (\mathbf{w}_i, \mathbf{w})_{\mathbf{V}_0} = f_i(\mathbf{w}) = (\mathbf{h}_i, \mathbf{w})_{\mathbf{V}_0}.$$

It follows that $P_i\mathbf{w}_i = \mathbf{h}_i$. □

2.3.2. *Link with the equilibrium gap method in a simple case*

Some connections exist between the Equilibrium Gap Method (EGM) and the Virtual Fields Method (VFM). In [41], it is shown that, at the discrete level, EGM and VFM are equivalent for a specific choice of virtual fields.

In certain simple cases, a direct connection can also be established between EGM and the VFM using the proposed virtual fields at the continuous level. Let us consider a very simple case of a single parameter and a single coefficient. In this situation, no projection onto $\mathbf{H}_i$ is needed. For instance, consider the reconstruction of $\alpha \in \mathbb{R}$ in the problem

$$\begin{cases} -\nabla \cdot \big((1 + \alpha\phi)\, \varepsilon(\mathbf{u})\big) = \mathbf{f}, & \text{in } \Omega, \\ \mathbf{u} = 0, & \text{on } \Gamma_D = \partial\Omega, \end{cases} \tag{23}$$

where ϕ is a given smooth, compactly supported scalar function. For the true parameter α, the solution $\mathbf{u}$ is assumed to belong to $\mathbf{V}_0 = H_0^1(\Omega)^d$. Choosing the scalar product in $\mathbf{V}_0$ as

$$\forall\ (\mathbf{q}, \mathbf{w}) \in \mathbf{V}_0 \times \mathbf{V}_0, \quad (\mathbf{q}, \mathbf{w})_{\mathbf{V}_0} = \int_\Omega \nabla\mathbf{q} : \nabla\mathbf{w}\, \mathrm{d}x,$$

the proposed virtual field $\mathbf{v} \in \mathbf{V}_0$, following Definition 1, satisfies the weak formulation

$$\int_\Omega \nabla\mathbf{v} : \nabla\mathbf{w}\, \mathrm{d}x = \int_\Omega \phi\, \varepsilon(\mathbf{u}) : \varepsilon(\mathbf{w})\, \mathrm{d}x, \quad \forall\, \mathbf{w} \in \mathbf{V}_0.$$

In strong form, $\mathbf{v}$ solves

$$\begin{cases} \Delta\mathbf{v} = \nabla \cdot \big(\phi\, \varepsilon(\mathbf{u})\big), & \text{in } \Omega, \\ \mathbf{v} = 0, & \text{on } \Gamma_D = \partial\Omega, \end{cases}$$

which yields

$$\mathbf{v} = -\Delta_0^{-1}\big(-\nabla \cdot \big(\phi\, \varepsilon(\mathbf{u})\big)\big) \in \mathbf{V}_0 = H_0^1(\Omega)^d, \tag{24}$$

where Δ_0^{-1} formally denotes the inverse of the Laplace operator with homogeneous Dirichlet boundary conditions. In fact, $\mathbf{v}$ as defined in (24) is the Riesz representative in $\mathbf{V}_0$ of the linear form $-\big(\nabla \cdot \big(\phi\, \varepsilon(\mathbf{u})\big)\big) \in (\mathbf{V}_0)'$. Importantly, it is well-defined without additional assumptions (even if ϕ is discontinuous). It can be shown that the EGM is equivalent to the VFM when the virtual field is chosen, assuming $\mathbf{u}$ is smooth, as

$$\mathbf{v} = -\nabla \cdot \big(\phi\, \varepsilon(\mathbf{u})\big) \in \mathbf{V}_0, \tag{25}$$

which is admissible since ϕ is smooth and compactly supported. Denoting $\mathbf{L}^2(\Omega) = L^2(\Omega)^d$, the equivalence between EGM and VFM with this particular virtual field arises from the fact that, in EGM, one solves

$$\alpha = \arg\min_{\widetilde{\alpha} \in \mathbb{R}} \big\| \nabla \cdot \big((1 + \widetilde{\alpha}\phi)\, \varepsilon(\mathbf{u})\big) + \mathbf{f} \big\|^2_{\mathbf{L}^2(\Omega)}.$$

Setting the gradient to zero leads to

$$\alpha = \frac{\big(\mathbf{f} + \nabla \cdot \varepsilon(\mathbf{u}), -\nabla \cdot \big(\phi\, \varepsilon(\mathbf{u})\big)\big)_{\mathbf{L}^2(\Omega)}}{\big\| \nabla \cdot \big(\phi\, \varepsilon(\mathbf{u})\big) \big\|^2_{\mathbf{L}^2(\Omega)}},$$

which corresponds exactly to (15) with (25) after integration by parts. This demonstrates that, in the simple case (23), under additional regularity assumptions, the virtual field proposed in Definition 1 is indeed the Riesz representative of the virtual field that naturally arises in EGM.

Overall, the method retains the same underlying idea of using equilibrium residuals, but it allows for proper treatment of cases where the solution is not necessarily smooth, accommodates various boundary conditions, and — since it is formulated at the continuous level — clearly distinguishes discretization errors from measurement noise.

2.3.3. *Parameter reconstruction from noisy data*

We assume access to data $\mathbf{u}^\delta$, representing displacement measurements that may be corrupted by noise. The parameter $\delta \geq 0$ quantifies the noise level in the data. Modeling errors are incorporated as uncertainties related to this noise level, and ℓ^δ denotes the counterpart of ℓ adapted to the noisy data. When $\delta = 0$, the data are assumed to be exact, and the corresponding noiseless displacement field, denoted by $\mathbf{u}^0$, is the solution to (9) associated with the coefficient $\theta^0(\mathbf{x}) = \sum_{j=1}^n \alpha_j^0 \phi_j(\mathbf{x})$. Our objective is to reconstruct an approximation θ^δ of the true parameter θ^0 using the noisy data $\mathbf{u}^\delta$. The reconstruction is sought in the form

$$\theta^\delta(\mathbf{x}) = \sum_{j=1}^n \alpha_j^\delta \phi_j(\mathbf{x}).$$

We keep the same notations as in the previous section. The matrix $\boldsymbol{A}$ is now constructed using the noisy displacement field $\mathbf{u}^\delta$ instead of $\mathbf{u}$, and is denoted by $\boldsymbol{A}^\delta$. The virtual fields are defined according to Definition 3 using $\mathbf{u}^\delta$ rather than $\mathbf{u}$. More precisely, we have the following.

Definition 7. *We define the virtual fields* $\{\mathbf{v}_i^\delta\}_i$ *by*

$$\mathbf{v}_i^\delta = \underset{\mathbf{v}\in\mathbf{H}_i^\delta,\ \|\mathbf{v}\|_{\mathbf{V}_0}\leq 1}{\arg\max} \quad f_i^\delta(\mathbf{v}), \tag{26}$$

where the continuous linear form f_i^δ *is defined as*

$$\begin{aligned} f_i^\delta : \mathbf{V}_0 &\longrightarrow \mathbb{R}, \\ \mathbf{v} &\longmapsto a(\phi_i, \mathbf{u}^\delta, \mathbf{v}), \end{aligned} \tag{27}$$

and the space $\mathbf{H}_i^\delta$ *is defined by*

$$\mathbf{H}_i^\delta := \left\{ \mathbf{v} \in \mathbf{K}_0 \;\middle|\; a(\phi_j, \mathbf{u}^\delta, \mathbf{v}) = 0 \text{ for all } j \neq i \right\}. \tag{28}$$

The coefficients $\{\alpha_i^\delta\}_{i=1}^n$ are then determined independently from the decoupled equations

$$\alpha_i^\delta \, a(\phi_i, \mathbf{u}^\delta, \mathbf{v}_i^\delta) = \ell^\delta(\mathbf{v}_i^\delta), \quad \text{for } i = 1, \ldots, n. \tag{29}$$

Remark 8. Numerically, the actual computation of the virtual fields is performed using a penalization method (see Section 4). An exact approach could be carried out using Lagrange multipliers; however, we choose the penalization strategy for its simplicity in terms of implementation. As a result, each virtual field is obtained by solving a linear variational problem (i.e., one PDE per virtual field). These PDEs include additional constraints, in particular the one ensuring that the matrix $\boldsymbol{A}^\delta$ is diagonal in the case of multiple coefficients. More precisely, the i-th virtual field satisfies, for $\beta \gg 1$,

$$(\mathbf{v}_i, \mathbf{w})_{\mathbf{V}_0} + \beta \sum_{j\neq i} f_j^\delta(\mathbf{v}_i) \, f_j^\delta(\mathbf{w}) = f_i^\delta(\mathbf{w}), \quad \forall\, \mathbf{w} \in \mathbf{V}_0.$$

Since β is large, for $j \neq i$ we have $f_i^\delta(\mathbf{v}_j) \approx 0$, hence taking $\mathbf{w} = \mathbf{v}_j$ with $j \neq i$, we obtain

$$(\mathbf{v}_i, \mathbf{v}_j)_{\mathbf{V}_0} + \beta \sum_{j\neq i} f_j^\delta(\mathbf{v}_i) \, f_j^\delta(\mathbf{v}_j) \approx 0.$$

2.3.4. *Stability analysis*

We now discuss the stability of the reconstruction with respect to noise in the data. Specifically, we aim to quantify the difference between the reconstructed parameters θ^δ, obtained from noisy measurements following the procedure outlined in the previous section, and the true parameter θ^0, corresponding to the noiseless case. To analyze the stability, we focus on the gap $\alpha_j^\delta - \alpha_j$ for each $1 \le j \le n$ which controls the difference $\theta_k^\delta - \theta_k^0$. For this purpose, we define $\chi^\delta := \mathbf{u}^\delta - \mathbf{u}^0$.

From Eq. (9), for each $1 \le i \le n$, we have

$$\sum_{j=1}^{n} \alpha_j^0 \, a(\phi_j, \mathbf{u}^0, \mathbf{v}_i^\delta) = \ell(\mathbf{v}_i^\delta).$$

which implies, since $\mathbf{v}_i^\delta \in \mathbf{H}_i^\delta$,

$$\begin{aligned} \alpha_i^0 \, a(\phi_i, \mathbf{u}^0, \mathbf{v}_i^\delta) &= \ell(\mathbf{v}_i^\delta) - \sum_{\substack{1 \le j \le n \\ j \ne i}} \alpha_j^0 \, a(\phi_j, \mathbf{u}^0, \mathbf{v}_i^\delta) \\ &= \ell(\mathbf{v}_i^\delta) + \sum_{\substack{1 \le j \le n \\ j \ne i}} \alpha_j^0 \, a(\phi_j, \chi^\delta, \mathbf{v}_i^\delta). \end{aligned} \tag{30}$$

By subtracting equation (30) from equation (29), we obtain

$$\alpha_i^\delta \, a(\phi_i, \mathbf{u}^\delta, \mathbf{v}_i^\delta) - \alpha_i^0 \, a(\phi_i, \mathbf{u}^0, \mathbf{v}_i^\delta) = \ell^\delta(\mathbf{v}_i^\delta) - \ell(\mathbf{v}_i^\delta) - \sum_{\substack{1 \le j \le n \\ j \ne i}} \alpha_j^0 \, a(\phi_j, \chi^\delta, \mathbf{v}_i^\delta).$$

Equivalently,

$$(\alpha_i^\delta - \alpha_i^0) \, a(\phi_i, \mathbf{u}^\delta, \mathbf{v}_i^\delta) = \ell^\delta(\mathbf{v}_i^\delta) - \ell(\mathbf{v}_i^\delta) - \sum_{1 \le j \le n} \alpha_j^0 \, a(\phi_j, \chi^\delta, \mathbf{v}_i^\delta).$$

We thus obtain the estimate

$$|\alpha_i^\delta - \alpha_i^0| \le \frac{1}{\left| a(\phi_i, \mathbf{u}^\delta, \mathbf{v}_i^\delta) \right|} \left(\|\ell^\delta - \ell\|_{\mathbf{V}'} + C_a \|\chi^\delta\|_{\mathbf{V}} \right),$$

where the constant C_a is defined in (4). This in turn implies that we have, for $q \in [1, +\infty]$,

$$\|\theta^\delta - \theta^0\|_{L^q(\Omega)} \le \left(\sum_{i=1}^{n} \frac{\|\phi_i\|_{L^q(\Omega)}}{\left| a(\phi_i, \mathbf{u}^\delta, \mathbf{v}_i^\delta) \right|} \right) \left(\|\ell^\delta - \ell\|_{\mathbf{V}'} + C_a \|\chi^\delta\|_{\mathbf{V}} \right).$$

This stability analysis shows that the reconstruction stability depends on the inverse of the diagonal entries of the matrix $\boldsymbol{A}^\delta$, which we have sought to minimize, as well as on the number of basis functions n. As $n \to \infty$, the stability constant may become unbounded. Moreover, if one of the virtual fields $\mathbf{v}_i$ is such that the corresponding diagonal term $a(\phi_i, \mathbf{u}^\delta, \mathbf{v}_i^\delta)$ vanishes, the stability constant is also unbounded. Otherwise, it remains bounded, provided that the diagonal terms stay uniformly away from zero. More precisely, we have shown the following theorem.

Theorem 9. *Assume that, for some $q \in [1, \infty]$, there exists a constant $C_q > 0$ such that, for sufficiently small δ,*

$$\sum_{i=1}^{n} \frac{\|\phi_i\|_{L^q(\Omega)}}{\left| a(\phi_i, \mathbf{u}^\delta, \mathbf{v}_i^\delta) \right|} \le C_q.$$

Then the reconstructed parameter θ^δ satisfies

$$\|\theta^\delta - \theta^0\|_{L^q(\Omega)} \le C_q \left(\|\ell^\delta - \ell\|_{\mathbf{V}'} + C_a \|\mathbf{u}^\delta - \mathbf{u}^0\|_{\mathbf{V}} \right),$$

where C_a is defined in (4).

2.4. *The multi-parameter case*

In this section, we consider the reconstruction of the mn coefficients $\{\alpha_{j,k}\}$ as defined in (6), which, according to Section 2.2, correspond to the solution of system (13).

2.4.1. *Definition and computation of optimal virtual fields*

We define the virtual fields such that the matrix $\boldsymbol{A}$ is diagonal. More precisely, for each $i \in \{1,\dots,mn\}$, we associate a unique pair of indices (k_i, j_i), so that:

$$\boldsymbol{A}_{ii} = a_{k_i}(\phi_{j_i,k_i}, \mathbf{u}, \mathbf{v}_i).$$

Each virtual field $\mathbf{v}_i$ is thus selected in the subspace:

$$\mathbf{H}_i := \left\{ \mathbf{v} \in \mathbf{K}_0 \;\middle|\; a_k(\phi_{j,k}, \mathbf{u}, \mathbf{v}) = 0 \text{ for all } (k,j) \neq (k_i, j_i) \right\}.$$

This construction ensures the independent recoverability of each coefficient $\alpha_{j_i}^{(k_i)}$ from the system. We note that $\mathbf{H}_i$ is a closed vector subspace of V, and hence a Hilbert space, endowed with the same inner product as V.

Definition 10 (Multi-parameter/multi-coefficient case). *We define the virtual fields* $\{\mathbf{v}_i\}_i$ *by*

$$\mathbf{v}_i = \underset{\mathbf{v}\in\mathbf{H}_i,\ \|\mathbf{v}\|_{\mathbf{V}_0}\leq 1}{\arg\max} f_i(\mathbf{v}), \tag{31}$$

where the continuous linear form f_i *is defined as*

$$\begin{aligned} f_i : \mathbf{V}_0 &\longrightarrow \mathbb{R}, \\ \mathbf{v} &\longmapsto a_{k_i}(\phi_{j_i,k_i}, \mathbf{u}, \mathbf{v}). \end{aligned} \tag{32}$$

We now address the computation of $\mathbf{v}_i$. The following theorem can be proved in the same way as in Section 2.3.1.

Theorem 11. *A solution to* (31) *is given by*

$$\mathbf{v}_i = \frac{\mathbf{h}_i}{\|\mathbf{h}_i\|_{\mathbf{V}_0}}, \quad \textit{with } (\mathbf{h}_i, \mathbf{w})_{\mathbf{V}_0} = f_i(\mathbf{w}),\ \forall\ \mathbf{w} \in \mathbf{H}_i.$$

2.4.2. *Parameter reconstruction from noisy data*

We assume access to data $\mathbf{u}^\delta$, representing displacement measurements possibly corrupted by noise. The parameter $\delta \geq 0$ quantifies the noise level in the data. Modeling errors are taken into account as uncertainties related to this noise level, and ℓ^δ denotes the counterpart of ℓ adapted to the noisy data. When $\delta = 0$, the data are assumed to be exact, and the corresponding noiseless displacement field, denoted by $\mathbf{u}^0$, is the solution to (7) associated with $\theta_k^0(\mathbf{x}) = \sum_{j=1}^n \alpha_{j,k}^0 \phi_{j,k}(\mathbf{x})$, for $1 \leq k \leq m$. Our goal is to reconstruct an approximation $\{\theta_k^\delta\}_{k=1}^m$ of the true parameters $\{\theta_k^0\}_{k=1}^m$ using the noisy data $\mathbf{u}^\delta$. The reconstruction is sought in the form

$$\theta_k^\delta(\mathbf{x}) = \sum_{i=1}^n \alpha_{i,k}^\delta \phi_{i,k}(\mathbf{x}), \quad \text{for } 1 \leq k \leq m.$$

We retain the same notations as in the previous section. The matrix $\boldsymbol{A}$ is now constructed using the noisy displacement field $\mathbf{u}^\delta$ instead of $\mathbf{u}$, and is denoted by $\boldsymbol{A}^\delta$. The virtual fields are defined according to Definition 10 using $\mathbf{u}^\delta$ rather than $\mathbf{u}$. The coefficients $\alpha_{j,k}^\delta$ are then recovered independently from the decoupled equations.

$$\alpha_{j_i,k_i}^\delta\, a_{k_i}(\phi_{j_i,k_i}, \mathbf{u}^\delta, \mathbf{v}_i^\delta) = \ell^\delta(\mathbf{v}_i^\delta), \quad \text{for } i = 1,\dots,mn. \tag{33}$$

2.4.3. *Stability analysis*

We now discuss the stability of the reconstruction with respect to noise in the data. Specifically, we aim to quantify the difference between the reconstructed parameters $\{\theta_k^\delta\}_{k=1}^m$, obtained from noisy measurements following the procedure outlined in the previous section, and the ideal reconstruction $\{\theta_k^0\}_{k=1}^m$, corresponding to the noiseless case. To analyze the stability, we focus on the gap $\alpha_{j,k}^\delta - \alpha_{j,k}^0$ for each $1 \le k \le m$ and $1 \le j \le n$, or equivalently $\alpha_{j_i,k_i}^\delta - \alpha_{j_i,k_i}^0$ for $1 \le i \le mn$.

Let us define $\chi^\delta := \mathbf{u}^\delta - \mathbf{u}^0$. From Eq. (7), for each $1 \le i \le mn$, we have

$$\sum_{k=1}^{m}\sum_{j=1}^{n} \alpha_{j,k}^0\, a_k(\phi_{j,k}, \mathbf{u}^0, \mathbf{v}_i^\delta) = \ell(\mathbf{v}_i^\delta),$$

which implies, since $\mathbf{v}_i^\delta \in \mathbf{H}_i^\delta$,

$$\begin{aligned}\alpha_{j_i,k_i}^0\, a_{k_i}(\phi_{j_i,k_i}, \mathbf{u}^0, \mathbf{v}_i^\delta) &= \ell(\mathbf{v}_i^\delta) - \sum_{\substack{1\le k\le m\\ 1\le j\le n\\ (j,k)\neq(j_i,k_i)}} \alpha_{j,k}^0\, a_k(\phi_{j,k}, \mathbf{u}^0, \mathbf{v}_i^\delta)\\ &= \ell(\mathbf{v}_i^\delta) + \sum_{\substack{1\le k\le m\\ 1\le j\le n\\ (j,k)\neq(j_i,k_i)}} \alpha_{j,k}^0\, a_k(\phi_{j,k}, \chi^\delta, \mathbf{v}_i^\delta).\end{aligned} \tag{34}$$

By subtracting equation (34) from equation (33), we obtain

$$\begin{aligned}&\alpha_{j_i,k_i}^\delta\, a_{k_i}(\phi_{j_i,k_i}, \mathbf{u}^\delta, \mathbf{v}_i^\delta) - \alpha_{j_i,k_i}^0\, a_{k_i}(\phi_{j_i,k_i}, \mathbf{u}^0, \mathbf{v}_i^\delta)\\ &\qquad = \ell^\delta(\mathbf{v}_i^\delta) - \ell(\mathbf{v}_i^\delta) - \sum_{\substack{1\le k\le m\\ 1\le j\le n\\ (j,k)\neq(j_i,k_i)}} \alpha_{j,k}^0\, a_k(\phi_{j,k}, \chi^\delta, \mathbf{v}_i^\delta).\end{aligned} \tag{35}$$

Equivalently,

$$(\alpha_{j_i,k_i}^\delta - \alpha_{j_i,k_i}^0)\, a_{k_i}(\phi_{j_i,k_i}, \mathbf{u}^\delta, \mathbf{v}_i^\delta) = \ell^\delta(\mathbf{v}_i^\delta) - \ell(\mathbf{v}_i^\delta) - \sum_{\substack{1\le k\le m\\ 1\le j\le n}} \alpha_{j,k}^0\, a_k(\phi_{j,k}, \chi^\delta, \mathbf{v}_i^\delta).$$

We thus obtain the estimate

$$|\alpha_{j_i,k_i}^\delta - \alpha_{j_i,k_i}^0| \le \frac{1}{\left|a_{k_i}(\phi_{j_i,k_i}, \mathbf{u}^\delta, \mathbf{v}_i^\delta)\right|}\left(\|\ell^\delta - \ell\|_{\mathbf{V}'} + C_a\|\chi^\delta\|_{\mathbf{V}}\right),$$

where the constant C_a is defined in (4).

This in turn implies that we have, for $q \in [1, +\infty]$, and all $k \in \{1, \dots, m\}$,

$$\|\theta_k^\delta - \theta_k^0\|_{L^q(\Omega)} \le \left(\sum_{j=1}^{n} \frac{\|\phi_{j,k}\|_{L^q(\Omega)}}{\left|a_k(\phi_{j,k}, \mathbf{u}^\delta, \mathbf{v}_{\mathscr{I}(j,k)}^\delta)\right|}\right)\left(\|\ell^\delta - \ell\|_{\mathbf{V}'} + C_a\,\|\chi^\delta\|_{\mathbf{V}}\right),$$

where $i = \mathscr{I}(j,k)$ is the index such that $j_i = j$ and $k_i = k$.

This stability analysis shows that the stability of the reconstruction depends on the inverse of the diagonal terms of the matrix $\boldsymbol{A}^\delta$, which we have sought to minimize, as well as on the product of the number of basis functions n and the number of parameters m. As mn tends to infinity, the stability constant may become unbounded. Moreover, if one of the virtual fields $\mathbf{v}_i$ is such that the corresponding diagonal term $a_k(\phi_{j,k}, \mathbf{u}^\delta, \mathbf{v}_{\mathscr{I}(j,k)}^\delta)$ vanishes, the stability constant is also unbounded. Otherwise, it remains bounded, provided the diagonal terms stay away from zero. More precisely, we have shown the following theorem.

Theorem 12. *Assume that, for sufficiently small δ, and for some $q \in [1,\infty]$, there exists a constant $C_q > 0$ such that for all $k \in \{1,\dots,m\}$,*

$$\left(\sum_{j=1}^{n} \frac{\|\phi_{j,k}\|_{L^q(\Omega)}}{\left| a_k(\phi_{j,k}, \mathbf{u}^\delta, \mathbf{v}^\delta_{\mathscr{I}(j,k)}) \right|} \right) \leq C_q.$$

Then each reconstructed parameter θ_k^δ, for $1 \leq k \leq m$, satisfies

$$\|\theta_k^\delta - \theta_k^0\|_{L^q(\Omega)} \leq C_q \big(\|\ell^\delta - \ell\|_{\mathbf{V}'} + C_a \|\mathbf{u}^\delta - \mathbf{u}^0\|_{\mathbf{V}} \big),$$

where C_a is defined in (4).

3. Extensions

We now discuss several extensions of the proposed approach, including its adaptation to incompressible or nearly incompressible materials, as well as its generalization to nonlinear hyperelastic models such as neo-Hookean formulations.

3.1. *The incompressible and nearly-incompressible case*

We now extend the formulation to the incompressible and nearly incompressible cases in linear elasticity. The starting point remains the virtual work principle (1), but the kinematic constraint

$$\nabla \cdot \mathbf{u} = 0 \quad \text{(incompressible case)}, \quad \text{or} \quad \nabla \cdot \mathbf{u} \approx 0 \quad \text{(nearly incompressible case)}$$

requires the introduction of an additional unknown.

The Cauchy stress tensor is decomposed into deviatoric and volumetric contributions,

$$\boldsymbol{\sigma} = \boldsymbol{\sigma}_{\text{dev}} + p\,\mathbf{I}, \tag{36}$$

where the scalar field p denotes the hydrostatic pressure, defined by

$$p = \frac{1}{d}\,\text{tr}(\boldsymbol{\sigma}). \tag{37}$$

Mathematically, p can be interpreted as a Lagrange multiplier associated with the incompressibility constraint. In the nearly incompressible case, p is not treated as an independent parameter of interest; it is typically set as

$$p = \lambda\,\text{div}(\mathbf{u}), \tag{38}$$

where λ is the first Lamé constant, assumed to be very large and not a parameter to be reconstructed.

With this decomposition, Eq. (1) reads

$$\int_\Omega \boldsymbol{\sigma}_{\text{dev}}(\mathbf{u}) : \boldsymbol{\varepsilon}(\mathbf{v})\,\mathrm{d}\Omega + \int_\Omega p\,\text{tr}\big(\boldsymbol{\varepsilon}(\mathbf{v})\big)\,\mathrm{d}\Omega = \int_{\Gamma_N} \mathbf{t}\cdot\mathbf{v}\,\mathrm{d}\Gamma + \int_\Omega \mathbf{f}\cdot\mathbf{v}\,\mathrm{d}\Omega, \quad \forall\, \mathbf{v} \in \mathbf{V}_0. \tag{39}$$

Due to the linearity of the constitutive law, we can assume that the following decomposition holds

$$\int_\Omega \boldsymbol{\sigma}_{\text{dev}}(\mathbf{u}) : \boldsymbol{\varepsilon}(\mathbf{v})\,\mathrm{d}\Omega = \sum_{k=1}^{m} a_k(\theta_k, \mathbf{u}, \mathbf{v}), \tag{40}$$

where the trilinear form $a_k : X_k \times \mathbf{V} \times \mathbf{V}_0 \to \mathbb{R}$ is defined by

$$a_k(\theta_k, \mathbf{u}, \mathbf{v}) = \int_\Omega \theta_k \big(\mathbb{C}_k : \boldsymbol{\varepsilon}(\mathbf{u}) \big) : \boldsymbol{\varepsilon}(\mathbf{v})\,\mathrm{d}\Omega. \tag{41}$$

Here, θ_k are the unknown elastic parameters to be identified (for instance, effective components of the anisotropic elasticity tensor) and belong to the finite-dimensional Banach space $X_k = \text{span}\{\phi_{1,k},\dots,\phi_{n,k}\} \subset L^\infty(\Omega)$, while $\mathbb{C}_k$ are known tensors representing the individual contribution of each parameter to the constitutive law.

Therefore, Eq. (39) can be rewritten in a compact operator form as

$$\sum_{k=1}^{m} a_k(\theta_k, \mathbf{u}, \mathbf{v}) + b(p, \mathbf{v}) = \ell(\mathbf{v}), \quad \forall\, \mathbf{v} \in \mathbf{V}_0, \tag{42}$$

where

$$b(p, \mathbf{v}) = \int_\Omega p \nabla \cdot \mathbf{v} \mathrm{d}\Omega, \qquad \ell(\mathbf{v}) = \int_{\Gamma_N} \mathbf{t} \cdot \mathbf{v} \mathrm{d}\Gamma + \int_\Omega \mathbf{f} \cdot \mathbf{v} \mathrm{d}\Omega.$$

In the inverse problem, we assume that the displacement field $\mathbf{u}$ is available from measurements, whereas the pressure field p is not directly accessible. Since p cannot be measured or independently reconstructed, it is convenient to eliminate its contribution from the variational formulation. Moreover, the load distribution $\mathbf{t}$ may also be unknown and is generally much more difficult to measure than displacements, as discussed in the previous section. To address these difficulties, we restrict the choice of virtual fields to those that eliminate both the pressure term and, when unknown, the traction term. More precisely, they are chosen in

$$\mathbf{K}_0 = \left\{ \mathbf{v} \in \mathbf{V}_0 \;\middle|\; \nabla \cdot \mathbf{v} = 0 \text{ and } \mathbf{T}\mathbf{v} = \mathbf{0} \text{ on } \Gamma_N \right\}, \tag{43}$$

where the matrix field $\mathbf{T} \in L^\infty(\Gamma_N)^{d \times d}$ is defined such that the virtual work associated with the traction $\mathbf{t}$ vanishes whenever $\mathbf{t}$ is unknown, as in the previous section.

Therefore, we have

$$b(p, \mathbf{v}) = 0 \quad \forall\, p \in L^2(\Omega),\ \forall\, \mathbf{v} \in \mathbf{K}_0,$$

and Eq. (42) reads

$$\sum_{k=1}^{m} a_k(\theta_k, \mathbf{u}, \mathbf{v}) = \ell(\mathbf{v}), \quad \forall\, \mathbf{v} \in \mathbf{K}_0. \tag{44}$$

The space $\mathbf{K}_0$ is the main difference compared to the compressible case (it involves the divergence-free constraint). All the results derived previously remain valid with this new choice of $\mathbf{K}_0$.

3.2. *Nonlinear models*

The method naturally extends to nonlinear mechanics, as long as the constitutive law is linear with respect to the parameters to be identified. For more complex constitutive laws, the method would need to be adapted. As an example, we consider nonlinear hyperelastic materials using neo-Hookean models, which are widely employed to describe the large-deformation behavior of soft tissues [44]. Although the mechanical response is nonlinear, the constitutive law retains a linear dependence on the material parameter, which allows the proposed identification strategy to be applied in this setting.

In the virtual work principle (1), the Cauchy stress tensor is decomposed according to the "decoupled" form of the constitutive law as

$$\boldsymbol{\sigma} = \boldsymbol{\sigma}_{\mathrm{dev}} + \boldsymbol{\sigma}_{\mathrm{vol}},$$

where the deviatoric part represents the shear response, while the volumetric part accounts for changes in volume. For neo-Hookean material, these contributions are given by

$$\boldsymbol{\sigma}_{\mathrm{dev}} = \frac{\mu}{J} \operatorname{dev}(\bar{\mathbf{B}}), \qquad \boldsymbol{\sigma}_{\mathrm{vol}} = -p\mathbf{I}$$

where

$$\mathbf{F} = \mathbf{I} + \nabla \mathbf{u}, \qquad \mathbf{B} = \mathbf{F}\mathbf{F}^\top, \qquad \bar{\mathbf{B}} = J^{-2/3}\mathbf{B}, \qquad J = \det(\mathbf{F}).$$

Here μ represents the shear modulus. The definition of p depends upon whether the solid material considered is compressible or incompressible.

For the principle of virtual work to be well defined, we assume that $\mathbf{u}$ has sufficient regularity and that J is bounded away from zero by a fixed constant c_0. In particular, we introduce the following assumption.

Assumptions 13. *The displacement field satisfies*

$$\mathbf{u} \in \mathbf{W}_{c_0} := \{\mathbf{u} \in W^{1,\infty}(\Omega)^d \mid \det(\mathbf{I} + \nabla \mathbf{u}) \geq c_0 > 0\},$$

for a fixed constant c_0.

Under these conditions, we have $\mathbf{F} = I + \nabla \mathbf{u} \in L^\infty(\Omega)^{d\times d}$, $J = \det(\mathbf{F}) \in L^\infty(\Omega)$, and $\mathbf{B} = \mathbf{F}\mathbf{F}^T \in L^\infty(\Omega)^{d\times d}$.

3.2.1. *Compressible case*

When one allows compressibility, one prescribes the volumetric response through a stored-energy function that depends on the Jacobian J, often choosing the volumetric energy for neo-Hookean materials,

$$W_{\text{vol}}(J) = \frac{\kappa}{4}(J^2 - 1 - 2\ln J),$$

where κ is the bulk modulus. Then differentiating with respect to J gives

$$p = -\frac{\partial W_{\text{vol}}}{\partial J} = -\frac{\kappa}{2}\left(J - \frac{1}{J}\right),$$

so that

$$\boldsymbol{\sigma}_{\text{vol}} = -p\,\mathbf{I} = \frac{\kappa}{2}\left(J - \frac{1}{J}\right)\mathbf{I}.$$

The virtual work equation (1) then reads

$$\int_\Omega \frac{\mu}{J^{5/3}}\left(\mathbf{B} - \frac{1}{d}\operatorname{tr}(\mathbf{B})\,\mathbf{I}\right) : \boldsymbol{\varepsilon}(\mathbf{v})\,\mathrm{d}\Omega + \int_\Omega \frac{\kappa}{2}\left(J - \frac{1}{J}\right)\operatorname{tr}\big(\boldsymbol{\varepsilon}(\mathbf{v})\big)\,\mathrm{d}\Omega = \int_{\Gamma_N} \mathbf{t}\cdot\mathbf{v}\,\mathrm{d}\Gamma + \int_\Omega \mathbf{f}\cdot\mathbf{v}\,\mathrm{d}\Omega, \tag{45}$$

for all $\mathbf{v} \in \mathbf{V}_0$ with $\mathbf{V}_0$ defined as in the previous sections.

In this compressible setting, our objective is to reconstruct simultaneously the shear modulus μ and the bulk-modulus parameter κ from the measured displacement fields.

The parameters μ and κ are sought in two known finite-dimensional spaces,

$$X_\mu = \operatorname{span}\{\phi_{1,\mu}, \ldots, \phi_{m,\mu}\} \subset L^\infty(\Omega)^m, \qquad X_\kappa = \operatorname{span}\{\phi_{1,\kappa}, \ldots, \phi_{n,\kappa}\} \subset L^\infty(\Omega)^n.$$

Accordingly, we introduce the expansions

$$\mu(\mathbf{x}) = \sum_{i=1}^m \mu_i\,\phi_{i,\mu}(\mathbf{x}), \qquad \kappa(\mathbf{x}) = \sum_{i=1}^n \kappa_i\,\phi_{i,\kappa}(\mathbf{x}).$$

With this decomposition, Eq. (45) becomes

$$\sum_{i=1}^m \mu_i\, a_\mu(\phi_{i,\mu}, \mathbf{u}, \mathbf{v}) + \sum_{i=1}^n \kappa_i\, a_\kappa(\phi_{i,\kappa}, \mathbf{u}, \mathbf{v}) = \ell(\mathbf{v}), \quad \forall\ \mathbf{v} \in \mathbf{V}_0. \tag{46}$$

The forms a_μ and a_κ are defined as

$$a_\mu \colon X_\mu \times \mathbf{W}_{c_0} \times \mathbf{V}_0 \longrightarrow \mathbb{R}, \quad a_\mu(\phi_{i,\mu}, \mathbf{u}, \mathbf{v}) = \int_\Omega \frac{\phi_{i,\mu}}{J^{5/3}}\left(\mathbf{B} - \frac{1}{d}\operatorname{tr}(\mathbf{B})\,\mathbf{I}\right) : \boldsymbol{\varepsilon}(\mathbf{v})\,\mathrm{d}\Omega,$$

and

$$a_\kappa \colon X_\kappa \times \mathbf{W}_{c_0} \times \mathbf{V}_0 \longrightarrow \mathbb{R}, \quad a_\kappa(\phi_{i,\kappa}, \mathbf{u}, \mathbf{v}) = \int_\Omega \frac{\phi_{i,\kappa}}{2}\left(J - \frac{1}{J}\right)\operatorname{tr}\big(\boldsymbol{\varepsilon}(\mathbf{v})\big)\,\mathrm{d}\Omega.$$

For fixed $\mathbf{u} \in \mathbf{W}_{c_0}$, the mappings

$$a_\mu(\cdot, \mathbf{u}, \cdot) \colon X_\mu \times \mathbf{V}_0 \longrightarrow \mathbb{R}, \qquad a_\kappa(\cdot, \mathbf{u}, \cdot) \colon X_\kappa \times \mathbf{V}_0 \longrightarrow \mathbb{R},$$

are continuous bilinear forms.

Choice of virtual fields. In what follows, we proceed similarly to the previous sections. We select exactly $m+n$ virtual fields, chosen in $\mathbf{K}_0$ defined in (10). With this choice, the global system is constructed as follows. The matrix $\boldsymbol{A} \in \mathbb{R}^{(m+n)\times(m+n)}$ is partitioned into two submatrices:

$$\boldsymbol{A} = \left[\boldsymbol{A}^{(1)}\, \boldsymbol{A}^{(2)}\right],$$

where $\boldsymbol{A}^{(1)} \in \mathbb{R}^{(m+n)\times m}$ and $\boldsymbol{A}^{(2)} \in \mathbb{R}^{(m+n)\times n}$ are given by

$$\boldsymbol{A}^{(1)}_{ij} = a_\mu(\phi_{j,\mu}, \mathbf{u}, \mathbf{v}_i), \quad 1 \le i \le m+n,\ 1 \le j \le m,$$

and

$$\boldsymbol{A}^{(2)}_{ij} = a_\kappa(\phi_{j,\kappa}, \mathbf{u}, \mathbf{v}_i), \quad 1 \le i \le m+n,\ 1 \le j \le n.$$

The right-hand side $\boldsymbol{\lambda} \in \mathbb{R}^{m+n}$ is defined as

$$\boldsymbol{\lambda}_i = \ell(\mathbf{v}_i), \quad 1 \le i \le m+n.$$

The unknown vector $\boldsymbol{\alpha} \in \mathbb{R}^{m+n}$ groups the coefficients for all parameters, namely

$$\boldsymbol{\alpha} = \begin{pmatrix} \boldsymbol{\alpha}^{(1)} \\ \boldsymbol{\alpha}^{(2)} \end{pmatrix}, \quad \text{where} \quad (\boldsymbol{\alpha}^{(1)})_j = \mu_j,\ 1 \le j \le m, \quad (\boldsymbol{\alpha}^{(2)})_j = \kappa_j,\ 1 \le j \le n.$$

The final system is compactly written as

$$\boldsymbol{A}\boldsymbol{\alpha} = \boldsymbol{\lambda}. \tag{47}$$

In analogy with the linear elasticity case, the virtual fields are constructed so as to make the matrix $\boldsymbol{A}$ diagonal and to maximize its diagonal entries over the unit ball of $\mathbf{V}_0$. More precisely, we have the following.

Definition 14. *For each $1 \le i \le m$, the virtual field $\mathbf{v}_i$ is defined by*

$$\mathbf{v}_i = \underset{\substack{\mathbf{v}\in\mathbf{H}_i^{(1)} \\ \|\mathbf{v}\|_{\mathbf{V}}\le 1}}{\arg\max}\ a_\mu(\phi_{i,\mu}, \mathbf{u}, \mathbf{v}),$$

where

$$\mathbf{H}_i^{(1)} := \left\{ \mathbf{v} \in \mathbf{K}_0 \;\middle|\; \begin{array}{ll} a_\mu(\phi_{j,\mu}, \mathbf{u}, \mathbf{v}) = 0 & \forall\ 1 \le j \le m,\ j \ne i, \\ a_\kappa(\phi_{j,\kappa}, \mathbf{u}, \mathbf{v}) = 0 & \forall\ 1 \le j \le n \end{array} \right\}.$$

Similarly, for each $m+1 \le i \le m+n$, the virtual field $\mathbf{v}_i$ is defined by

$$\mathbf{v}_i = \underset{\substack{\mathbf{v}\in\mathbf{H}_i^{(2)} \\ \|\mathbf{v}\|_{\mathbf{V}}\le 1}}{\arg\max}\ a_\kappa(\phi_{i-m,\kappa}, \mathbf{u}, \mathbf{v}),$$

where

$$\mathbf{H}_i^{(2)} := \left\{ \mathbf{v} \in \mathbf{K}_0 \;\middle|\; \begin{array}{ll} a_\mu(\phi_{j,\mu}, \mathbf{u}, \mathbf{v}) = 0 & \forall\ 1 \le j \le m, \\ a_\kappa(\phi_{j,\kappa}, \mathbf{u}, \mathbf{v}) = 0 & \forall\ 1 \le j \le n,\ j \ne i-m \end{array} \right\}.$$

Remark 15. Several alternative choices of virtual fields have been proposed in the nonlinear setting; see, for instance, [42,43]. However, conducting a rigorous mathematical analysis of these approaches is not straightforward. Nevertheless, notable similarities can be identified.

In the case of homogeneous parameters, the equilibrium equation can be written as

$$-\mu\nabla\cdot\boldsymbol{\sigma}_\mu - \kappa\nabla\cdot\boldsymbol{\sigma}_\kappa = \mathbf{f}, \quad \boldsymbol{\sigma}_\mu = \frac{\partial\boldsymbol{\sigma}}{\partial\mu}, \quad \boldsymbol{\sigma}_\kappa = \frac{\partial\boldsymbol{\sigma}}{\partial\kappa}.$$

where $\boldsymbol{\sigma}_\mu$ and $\boldsymbol{\sigma}_\kappa$ now depend only on the deformation field $\mathbf{F}$.

The proposed virtual fields $\mathbf{v}_1$ and $\mathbf{v}_2$, following Definition 14, are defined as the projections of $\mathbf{w}_1$ and $\mathbf{w}_2$ onto

$$\mathbf{H}_1 = \left\{\mathbf{v}\in\mathbf{V}_0 \,:\, \left(\boldsymbol{\sigma}_\kappa : \boldsymbol{\varepsilon}(\mathbf{v})\right)_{L^2(\Omega)} = 0\right\}, \qquad \mathbf{H}_2 = \left\{\mathbf{v}\in\mathbf{V}_0 \,:\, \left(\boldsymbol{\sigma}_\mu : \boldsymbol{\varepsilon}(\mathbf{v})\right)_{L^2(\Omega)} = 0\right\},$$

where, assuming $\Gamma_D = \partial\Omega$,

$$\begin{cases} \Delta \mathbf{w}_1 = \nabla \cdot \boldsymbol{\sigma}_\mu & \text{in } \Omega, \\ \mathbf{w}_1 = \mathbf{0} & \text{on } \Gamma_D, \end{cases} \quad \text{and} \quad \begin{cases} \Delta \mathbf{w}_2 = \nabla \cdot \boldsymbol{\sigma}_\kappa & \text{in } \Omega, \\ \mathbf{w}_2 = \mathbf{0} & \text{on } \Gamma_D. \end{cases}$$

The fields $\mathbf{w}_1$ and $\mathbf{w}_2$ are closely related to the virtual fields proposed in [43]. In their work, the authors introduce virtual fields $\mathbf{v}_1$ and $\mathbf{v}_2$ in $\mathbf{V}_0$ belonging to the class

$$\begin{cases} \nabla \cdot \big(\mathbb{L} : \varepsilon(\mathbf{v}_1)\big) = \nabla \cdot \boldsymbol{\sigma}_\mu & \text{in } \Omega, \\ \mathbf{v}_1 = \mathbf{0} & \text{on } \Gamma_D, \end{cases} \quad \text{and} \quad \begin{cases} \nabla \cdot \big(\mathbb{L} : \varepsilon(\mathbf{v}_2)\big) = \nabla \cdot \boldsymbol{\sigma}_\kappa & \text{in } \Omega, \\ \mathbf{v}_2 = \mathbf{0} & \text{on } \Gamma_D, \end{cases}$$

where $\mathbb{L}$ is a fourth-order tensor. The main differences lie, first, in the use of the operator $-\nabla \cdot \big(\mathbb{L} : \varepsilon(\cdot)\big)$ instead of the Laplacian $-\Delta$, which, in our framework, corresponds to a different choice of scalar product in $\mathbf{V}_0$ (provided that $\mathbb{L}$ satisfies the usual symmetry and positivity properties); and second, in the fact that they do not aim to construct a diagonal matrix $\boldsymbol{A}^\delta$.

Parameter reconstruction from noisy data. We consider noisy displacement measurements $\mathbf{u}^\delta \in \mathbf{W}_{c_0}$, where $\delta \geq 0$ denotes the noise level. The quantity ℓ^δ denotes the noisy counterpart of the load functional ℓ, incorporating both measurement and modeling uncertainties. When $\delta = 0$, the data are assumed to be exact. The corresponding displacement field, denoted by $\mathbf{u}^0$, is the solution of (45) associated with the exact material parameters (μ^0, κ^0).

In the presence of noise, all ingredients of the identification procedure are constructed from $\mathbf{u}^\delta$. In particular, the matrix $\boldsymbol{A}^\delta$ is built using the noisy displacement field, and the virtual fields are those from Definition 14 with $\mathbf{u}$ replaced by $\mathbf{u}^\delta$. The coefficients $\{\alpha_i^\delta\}_{i=1}^{m+n}$ are then determined independently, thanks to the diagonal structure of $\boldsymbol{A}^\delta$, from the decoupled equations

$$\begin{cases} \mu_i^\delta \, a_\mu(\phi_{i,\mu}, \mathbf{u}^\delta, \mathbf{v}_i^\delta) = \ell^\delta(\mathbf{v}_i^\delta), & 1 \leq i \leq m, \\ \kappa_i^\delta \, a_\kappa(\phi_{i,\kappa}, \mathbf{u}^\delta, \mathbf{v}_{i+m}^\delta) = \ell^\delta(\mathbf{v}_{i+m}^\delta), & 1 \leq i \leq n. \end{cases}$$

Thus, the parameters are reconstructed as

$$\mu^\delta(\mathbf{x}) = \sum_{i=1}^{m} \mu_i^\delta \, \phi_{i,\mu}(\mathbf{x}), \qquad \kappa^\delta(\mathbf{x}) = \sum_{i=1}^{n} \kappa_i^\delta \, \phi_{i,\kappa}(\mathbf{x}).$$

3.2.2. *Incompressible case*

At the incompressible limit ($\kappa \to +\infty$, $J \to 1$), the volumetric stress cannot be defined through a constitutive law. It is instead given by

$$\boldsymbol{\sigma}_{\text{vol}} = -p\,\mathbf{I}, \qquad J = 1,$$

where p is interpreted as a Lagrange multiplier associated with the incompressibility constraint $J = 1$. The deviatoric part of the stress then simplifies to

$$\boldsymbol{\sigma}_{\text{dev}} = \mu \, \text{dev}(\mathbf{B}),$$

since $\overline{\mathbf{B}} = \mathbf{B}$ for incompressible motions. The principle of virtual work (1) then reads

$$\int_\Omega \mu \left(\mathbf{B} - \frac{1}{d} \operatorname{tr}(\mathbf{B}) \mathbf{I} \right) : \boldsymbol{\varepsilon}(\mathbf{v}) \, \mathrm{d}\Omega - \int_\Omega p \operatorname{tr}\big(\boldsymbol{\varepsilon}(\mathbf{v})\big) \, \mathrm{d}\Omega = \int_{\Gamma_N} \mathbf{t} \cdot \mathbf{v} \, \mathrm{d}\Gamma + \int_\Omega \mathbf{f} \cdot \mathbf{v} \, \mathrm{d}\Omega. \tag{48}$$

In the incompressible case, the objective reduces to reconstructing the shear modulus μ only. Using the same notation as in the compressible case, Eq. (48) becomes

$$\sum_{i=1}^{m} \mu_i \, a_\mu(\phi_{i,\mu}, \mathbf{u}, \mathbf{v}) + b(p, \mathbf{v}) = \ell(\mathbf{v}), \qquad \forall \ \mathbf{v} \in \mathbf{V}_0, \tag{49}$$

where the bilinear form associated with the incompressibility constraint is

$$b(p, \mathbf{v}) = -\int_\Omega p \, \nabla \cdot \mathbf{v} \, \mathrm{d}\Omega.$$

Similarly to what was done in Section 3.1, since the pressure p and the traction $\mathbf{t}$ are often not accessible, we restrict the choice of virtual fields to those that eliminate both the pressure term and, when unknown, the traction term. More precisely, the virtual fields are chosen in $\mathbf{K}_0$, defined in (43). The definition of the virtual fields and the construction of the decoupled identification system follow the same strategy as in the compressible case, with the only modification occurring in $\mathbf{K}_0$.

4. Illustrative numerical examples

We now demonstrate the effectiveness and flexibility of the reconstruction method through two applications and a series of numerical experiments. The first application concerns isotropic, nearly incompressible linear elasticity, while the second focuses on compressible, transversely isotropic linear elasticity.

4.1. *Isotropic nearly-incompressible linear medium*

In this section, we consider isotropic nearly-incompressible elasticity in the context of time-harmonic elastography. At an angular frequency ω, the displacement field $\mathbf{u}$ satisfies

$$\begin{cases} \nabla\cdot\boldsymbol{\sigma}+\mathbf{f}=\mathbf{0} & \text{in } \Omega,\\ \boldsymbol{\sigma}=\mathbb{C}:\boldsymbol{\varepsilon}(\mathbf{u}) & \text{in } \Omega,\\ \mathbf{u}=\mathbf{0} & \text{on } \Gamma_D,\\ \boldsymbol{\sigma}\cdot\boldsymbol{n}=\mathbf{t} & \text{on } \Gamma_N. \end{cases} \tag{50}$$

The elasticity tensor $\mathbb{C}$ is defined as

$$\mathbb{C}=\lambda\,\mathbf{I}\otimes\mathbf{I}+2\mu\,\mathbb{I},$$

where μ and λ denote the second (i.e., shear) and first Lamé coefficients, respectively. Here, $\mathbf{I}$ and $\mathbb{I}$ represent the second- and fourth-order identity tensors, with components $\mathbf{I}_{ij}=\delta_{ij}$ and $\mathbb{I}_{ijkl}=\delta_{ik}\delta_{jl}$. The body force field $\mathbf{f}$ corresponds to the inertial term,

$$\mathbf{f}=-\rho\omega^2\mathbf{u},$$

where ρ denotes the mass density.

Substituting these expressions into the virtual work principle (1), we obtain

$$\int_\Omega 2\mu\boldsymbol{\varepsilon}(\mathbf{u}):\boldsymbol{\varepsilon}(\mathbf{v})\,\mathrm{d}x+\int_\Omega\lambda\nabla\cdot\mathbf{u}\nabla\cdot\mathbf{v}\,\mathrm{d}x=\int_{\Gamma_N}\mathbf{t}\cdot\mathbf{v}\,\mathrm{d}\Gamma+\int_\Omega\rho\omega^2\mathbf{u}\cdot\mathbf{v}\,\mathrm{d}\Omega, \tag{51}$$

for any virtual field $\mathbf{v}\in\mathbf{V}_0$.

In the nearly-incompressible isotropic elasticity setting, the virtual work principle leads to a Stokes-like formulation:

$$\int_\Omega 2\mu\boldsymbol{\varepsilon}(\mathbf{u}):\boldsymbol{\varepsilon}(\mathbf{v})\,\mathrm{d}\Omega+\int_\Omega p\,\nabla\cdot\mathbf{v}\,\mathrm{d}\Omega=\int_{\Gamma_N}\mathbf{t}\cdot\mathbf{v}\,\mathrm{d}\Gamma+\int_\Omega\rho\omega^2\mathbf{u}\cdot\mathbf{v}\,\mathrm{d}\Omega, \tag{52}$$

for any virtual field $\mathbf{v}\in\mathbf{V}_0$. Using (52), μ satisfies a general variational form:

$$a(\mu,\mathbf{u},\mathbf{v})+b(p,\mathbf{v})=\ell(\mathbf{v}),\quad \text{for any } \mathbf{v}\in\mathbf{V}_0,$$

where

$$a(\mu,\mathbf{u},\mathbf{v})=\int_\Omega 2\mu\,\boldsymbol{\varepsilon}(\mathbf{u}):\boldsymbol{\varepsilon}(\mathbf{v})\,\mathrm{d}\Omega,\qquad b(p,\mathbf{v})=\int_\Omega p\,\nabla\cdot\mathbf{v}\,\mathrm{d}\Omega,$$

and

$$\ell(\mathbf{v})=\int_{\Gamma_N}\mathbf{t}\cdot\mathbf{v}\,\mathrm{d}\Gamma+\int_\Omega\rho\omega^2\mathbf{u}\cdot\mathbf{v}\,\mathrm{d}\Omega.$$

We aim to reconstruct the shear modulus μ, which is sought in the form

$$\mu(\mathbf{x}) = \sum_{i=1}^{n} \alpha_i \phi_i(\mathbf{x}),$$

where the functions ϕ_i are known.

Stability estimate. The choice of virtual fields follows the approach introduced in Sections 2 and 3.1. Let $\mathbf{u}^\delta$ denote the noisy displacement data and $\mathbf{u}^0$ the noise-free displacement field, solution to (50) associated with the true shear modulus $\mu^0(\mathbf{x}) = \sum_{j=1}^{n} \alpha_j^0 \phi_j(\mathbf{x})$. Let μ^δ denote its reconstruction from $\mathbf{u}^\delta$, with corresponding coefficients $\{\alpha_i^\delta\}_{i=1}^n$. Therefore, we have the following stability estimate (see Section 2.3.4).

Corollary 16. *Assume that, for some $q \in [1,\infty]$, there exists a constant $C_q > 0$ such that, for sufficiently small δ,*

$$\sum_{i=1}^{n} \frac{\|\phi_i\|_{L^q(\Omega)}}{\left|a(\phi_i, \mathbf{u}^\delta, \mathbf{v}_i^\delta)\right|} \leq C_q.$$

Then, the reconstructed parameter μ^δ satisfies

$$\|\mu^\delta - \mu^0\|_{L^q(\Omega)} \leq C\big(C_q, \rho, \omega, \|\mu^0\|_{L^\infty(\Omega)}\big)\|\mathbf{u}^\delta - \mathbf{u}^0\|_{\mathbf{V}}.$$

The proof follows directly from Theorem 9, noting that in this context, the functional ℓ^δ is given by

$$\ell^\delta(\mathbf{v}) = \int_{\Gamma_N} \mathbf{t}\cdot\mathbf{v}\,\mathrm{d}\Gamma + \int_\Omega \rho\omega^2 \mathbf{u}^\delta \cdot \mathbf{v}\,\mathrm{d}\Omega,$$

and that the constant C_a defined in (4) can be chosen as $2\|\mu^0\|_{L^\infty(\Omega)}$.

Numerical implementation. We consider a two-dimensional domain $\Omega = [0,1]^2$ and investigate several shear modulus distributions. For each case, the direct problem (50) is solved using the boundary conditions described below, with a finite element discretization on a mesh of size $h = 1/100$. To simulate realistic measurement errors, deterministic noise is added to the computed displacement field in a reproducible manner. The noisy displacement field is defined as

$$\mathbf{u}^\delta(\boldsymbol{x}) = \mathbf{u}^0(\boldsymbol{x}) + \delta\|\mathbf{u}^0\|_{H^1(\Omega)} \sum_{r=0}^{R} \frac{r}{R} \cos\left(2\pi \frac{r}{R} \frac{\boldsymbol{x}}{\sqrt{\delta}} \cdot \boldsymbol{e}_1\right) \cos\left(2\pi \frac{r}{R} \frac{\boldsymbol{x}}{\sqrt{\delta}} \cdot \boldsymbol{e}_2\right)(\boldsymbol{e}_1 + \boldsymbol{e}_2), \tag{53}$$

where $R = 10$ and $\mathbf{u}^0$ denotes the exact displacement field and δ controls the noise amplitude. The relative noise level is quantified in the H^1-norm as

$$\text{Relative noise level} = \frac{\|\mathbf{u}^0 - \mathbf{u}^\delta\|_{H^1(\Omega)}}{\|\mathbf{u}^0\|_{H^1(\Omega)}} \times 100\%.$$

For simplicity, we assume that the exact shear modulus μ^0 can be written as

$$\mu^0(\mathbf{x}) = 1 + \sum_{i=1}^{n} \alpha_i^0 \phi_i(\mathbf{x}),$$

where n denotes the number of inclusions. We then proceed to the reconstruction of the shear modulus.

Algorithm 1 summarizes the main steps of the VFM-based reconstruction procedure. The relative error of reconstruction is then computed as

$$\text{Relative error} = \frac{\|\mu^0 - \mu^\delta\|_{L^2(\Omega)}}{\|\mu^0\|_{L^2(\Omega)}} \times 100\%,$$

where μ^δ denote reconstructed shear modulus field.

Algorithm 1: VFM-Based Reconstruction of $\mu^\delta = 1 + \sum_{i=1}^n \alpha_i^\delta \phi_i(\mathbf{x})$ from $\mathbf{u}^\delta$

Input: noisy displacement field $\mathbf{u}^\delta$, affine space spanned by $\{\phi_i\}_{i=1}^n$

Output: reconstructed shear modulus μ^δ

1 **for** $i = 1$ **to** n **do**

2 Find $(\mathbf{h}_i, p) \in \mathbf{V}_0 \times L^2(\Omega)$ such that

$$\int_\Omega \nabla \mathbf{h}_i : \nabla \mathbf{w} \, \mathrm{d}x + \beta \sum_{\substack{j=1 \\ j \neq i}}^{n} \left(\int_\Omega \phi_j \boldsymbol{\varepsilon}(\mathbf{u}^\delta) : \boldsymbol{\varepsilon}(\mathbf{h}_i) \, \mathrm{d}x \right) \left(\int_\Omega \phi_j \boldsymbol{\varepsilon}(\mathbf{u}^\delta) : \boldsymbol{\varepsilon}(\mathbf{w}) \, \mathrm{d}x \right) + \int_\Omega p \nabla \cdot \mathbf{w} \, \mathrm{d}x = \int_\Omega \phi_i \boldsymbol{\varepsilon}(\mathbf{u}^\delta) : \boldsymbol{\varepsilon}(\mathbf{w}) \, \mathrm{d}x,$$

$$\int_\Omega q \nabla \cdot \mathbf{h}_i \, \mathrm{d}x = 0,$$

for all $(\mathbf{w}, q) \in \mathbf{V} \times L^2(\Omega)$, with $\beta \gg 1$.

3 Update row i of $\boldsymbol{A}^\delta \in \mathbb{R}^{n \times n}$:

$$A_{i,j}^\delta = \int_\Omega 2\phi_j \boldsymbol{\varepsilon}(\mathbf{u}^\delta) : \boldsymbol{\varepsilon}(\mathbf{h}_i) \, \mathrm{d}x, \quad j = 1, \ldots, n.$$

4 Update entry i of $\boldsymbol{\lambda} \in \mathbb{R}^n$:

$$\lambda_i^\delta = \int_\Omega \rho \omega^2 \mathbf{u}^\delta \cdot \mathbf{h}_i \, \mathrm{d}\Omega - \int_\Omega 2\boldsymbol{\varepsilon}(\mathbf{u}^\delta) : \boldsymbol{\varepsilon}(\mathbf{h}_i) \, \mathrm{d}x.$$

5 Solve the linear system

$$\boldsymbol{A}^\delta \boldsymbol{\alpha}^\delta = \boldsymbol{\lambda}^\delta,$$

and compute the reconstructed shear modulus

$$\mu^\delta(\mathbf{x}) = 1 + \sum_{i=1}^n \alpha_i^\delta \phi_i(\mathbf{x}).$$

6 **return** μ^δ

In the following, we present the reconstruction results to evaluate the performance of the proposed approach. In the first case, we consider disjoint inclusions, while in the second case, overlapping inclusions are studied.

4.1.1. *Disjoint inclusions*

Here, we consider phantoms with piecewise constant heterogeneous shear moduli, as illustrated in Figure 3, where the subregions are disjoint and known a priori.

A comparative study is conducted using three types of virtual fields to evaluate the performance of the proposed approach.

Type 1: Optimal VF. The virtual field proposed in this work.

Type 2: Curl-based VF. A virtual field defined as the curl of a vector field,

$$\mathbf{v}^* = \nabla \times \mathbf{F}, \tag{54}$$

where $\mathbf{F}$ is a nonzero vector field and $\mathbf{v}^*$ is required to be kinematically admissible.

Type 3: Solution-based VF. A virtual field obtained by solving the forward incompressible elasticity problem with a homogeneous modulus. More precisely, for a given source term $\mathbf{f} \in L^2(\Omega)^2$ we seek a pair $(\mathbf{v}^*, p^*) \in \mathbf{V}_0 \times L^2(\Omega)$ satisfying

$$\begin{cases} \nabla \cdot \left(\boldsymbol{\varepsilon}(\mathbf{v}^*) \right) + \nabla p^* = \mathbf{f} & \text{in } \Omega, \\ \nabla \cdot \mathbf{v}^* = 0 & \text{in } \Omega, \end{cases} \tag{55}$$

for different boundary conditions (see Figure 4). The latter two types were introduced in [45]. In both cases, the resulting displacement fields automatically satisfy the incompressibility constraint.

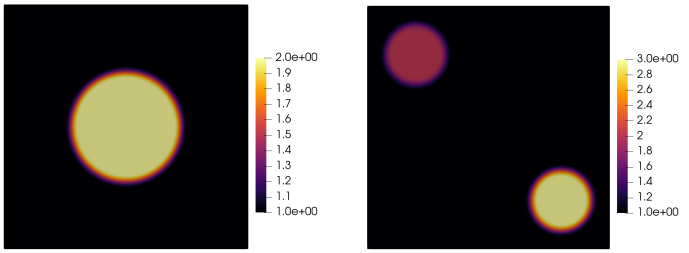

Figure 3. Examples of shear modulus phantoms: (a) μ_1 with a single inclusion, and (b) μ_2 with two inclusions.

For all three types of virtual fields, n different virtual fields are required to identify the n coefficients corresponding to the n inclusions. For the first type, all n virtual fields can be constructed from a single displacement field. In contrast, for Types 2 and 3, by definition, n distinct boundary conditions are needed to generate the n virtual fields. As an illustrative example, we first consider the case with the bottom boundary clamped (zero displacement), as shown in Figure 4, while treating the top-edge traction as unknown. To eliminate the virtual work contribution from this unknown loading, we impose zero vertical components for the virtual fields in Figures 4(a)–(b) and zero horizontal components for the virtual field in Figure 4(c) along the top boundary. The space of virtual fields $\mathbf{V}_0$ accounts for these additional constraints.

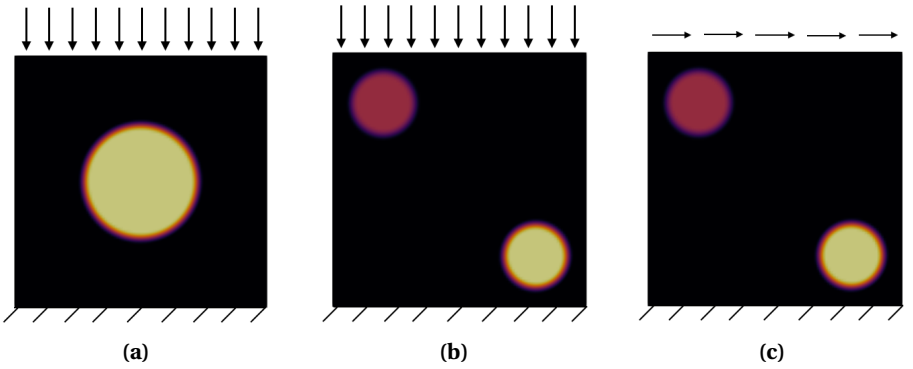

Figure 4. (a) One type of boundary condition used to generate a virtual field for the first model. (b)–(c) Two different boundary conditions used to generate virtual fields of Types 2 and 3, respectively, for the second model.

One single inclusion. For the first test case (μ_1, Figure 3(a)), we consider the domain illustrated in Figure 4(a) (see [45]).

The Type 1 virtual field, defined as in Section 3.1, is given by

$$\mathbf{v}^{(1)} = \underset{\mathbf{v}\in\mathbf{K}_0,\ \|\mathbf{v}\|_{H^1(\Omega)}\leq 1}{\arg\max} \ a(\phi_1, \mathbf{u}^\delta, \mathbf{v}),$$

where ϕ_1 denotes the inclusion function, and the set $\mathbf{K}_0$ is defined as

$$\mathbf{K}_0 = \left\{\mathbf{v}\in\mathbf{V}_0 \,\middle|\, \nabla\cdot\mathbf{v} = 0 \text{ and } (\mathbf{v}\cdot\mathbf{e}_2)(\cdot,1) = 0\right\},$$

with

$$\mathbf{V}_0 = \left\{ \mathbf{v} \in H^1(\Omega)^2 \;\middle|\; \mathbf{v}(\cdot, 0) = \mathbf{0} \right\}.$$

The Type 2 virtual field, defined by Eq. (54), also belongs to $\mathbf{K}_0$. It is explicitly given by

$$\mathbf{v}^{(2)}(x, y) = \begin{pmatrix} -xy(3y-2) \\ y^2(y-1) \\ 0 \end{pmatrix}.$$

Finally, the Type 3 virtual field, also belongs to $\mathbf{K}_0$, denoted $\mathbf{v}^{(3)}$, is obtained by solving Eq. (55) in $\left\{ \mathbf{v} \in \mathbf{V}_0 \;\middle|\; (\mathbf{v} \cdot \mathbf{e}_2)(\cdot, 1) = 0 \right\} \times L^2(\Omega)$ with an arbitrarily chosen source term; here,

$$\mathbf{f}(x, y) = \begin{pmatrix} x\cos\big(10(x+y)\big) \\ x\sin\big(10(x+y)\big) \end{pmatrix}.$$

Figure 5(a) presents the relative error in the reconstructed shear modulus of the inclusion versus noise level for all three virtual field types.

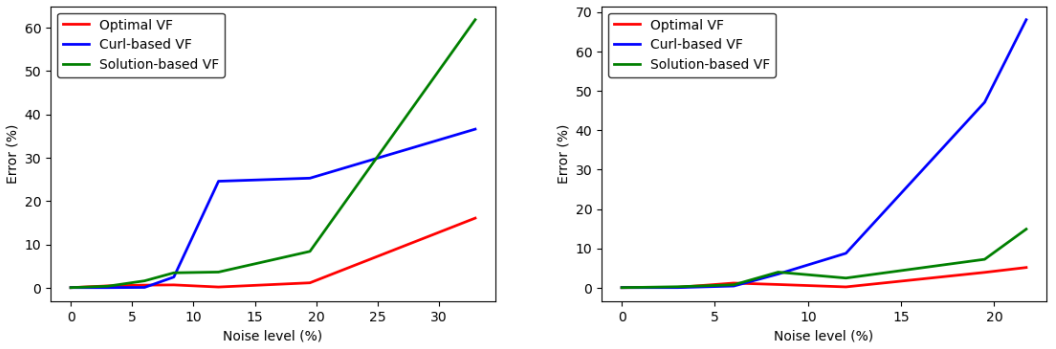

(a) **(b)**

Figure 5. Relative error for two different target shear modulus distributions under varying noise levels, using the three types of virtual fields: (a) first model, (b) second model.

Two disjoint inclusions. For the second test case (μ_2, Figure 3(b)), we use the displacement field corresponding to the boundary conditions shown in Figure 4(b) to compute the proposed virtual fields.

The two virtual fields of Type 1 are given by

$$\mathbf{v}_1^{(1)} = \underset{\mathbf{v} \in H_1,\ \|\mathbf{v}\|_{H^1(\Omega)} \leq 1}{\arg\max} \; a(\phi_1, \mathbf{u}^\delta, \mathbf{v}), \qquad \mathbf{v}_2^{(1)} = \underset{\mathbf{v} \in H_2,\ \|\mathbf{v}\|_{H^1(\Omega)} \leq 1}{\arg\max} \; a(\phi_2, \mathbf{u}^\delta, \mathbf{v}),$$

where ϕ_1 and ϕ_2 denote the two inclusion functions, and the sets H_1 and H_2 are defined as

$$H_1 = \left\{ \mathbf{v} \in \mathbf{K}_0 \;\middle|\; a(\phi_2, \mathbf{u}^\delta, \mathbf{v}) = 0 \right\},$$

and

$$H_2 = \left\{ \mathbf{v} \in \mathbf{K}_0 \;\middle|\; a(\phi_1, \mathbf{u}^\delta, \mathbf{v}) = 0 \right\}.$$

The two virtual fields of Type 2 are explicitly given by

$$\mathbf{v}_1^{(2)}(x, y) = \begin{pmatrix} -xy(3y-2) \\ y^2(y-1) \\ 0 \end{pmatrix}, \qquad \mathbf{v}_2^{(2)}(x, y) = \begin{pmatrix} xy(y-1) \\ -\dfrac{y^3}{3} + \dfrac{y^2}{2} \\ 0 \end{pmatrix}.$$

The corresponding Type 3 virtual fields, denoted $\mathbf{v}_1^{(3)}$ and $\mathbf{v}_2^{(3)}$, are obtained by solving Eq. (55) subject to the following boundary conditions respectively:

$$\begin{cases} \mathbf{v}_1^{(3)}(\cdot,0) = \mathbf{0}, \\ (\mathbf{v}_1^{(3)} \cdot \mathbf{e}_2)(\cdot,1) = 0, \end{cases} \qquad \begin{cases} \mathbf{v}_2^{(3)}(\cdot,0) = \mathbf{0}, \\ (\mathbf{v}_2^{(3)} \cdot \mathbf{e}_1)(\cdot,1) = 0. \end{cases}$$

Figure 5(b) shows the relative error in the reconstructed shear modulus within the inclusion, as a function of the noise level, for each of the three types of virtual fields.

Discussion. The results in Figure 5 demonstrate that the proposed virtual fields (Optimal VF) successfully recover the target shear modulus with high precision. This experimental validation confirms the theoretical stability estimate with respect to noise, measured in the H^1-norm of the displacement fields. For the first configuration (Figure 5(a)), where a single inclusion is considered, all three types of virtual fields yield relatively small errors at low noise levels. However, as the noise increases, Type 1 clearly outperforms the other two: its reconstruction error remains significantly lower, while errors from Type 2 (curl-based) and Type 3 (forward solution-based) increase more rapidly. This trend becomes even more pronounced in the second configuration (Figure 5(b)), involving two inclusions. Even under substantial noise, the Type 1 virtual field consistently delivers more stable and accurate reconstructions. In contrast, both Type 2 and Type 3 exhibit a sharp deterioration in performance as the noise level grows, confirming the practical advantage of our proposed optimal virtual field approach.

4.1.2. *Overlapping inclusions*

The method also performs well in cases where the inclusions are not disjoint. To demonstrate this, we present numerical results for such configurations. Specifically, we consider one example with three overlapping circular inclusions (see Figure 6(a)), and another case where the geometry is only partially known. In the latter, we assume the presence of two circular inclusions (see Figure 6(b)), but their exact radii are unknown. Instead, we consider a set of candidate circular inclusions with different radii (see Figure 6(c)).

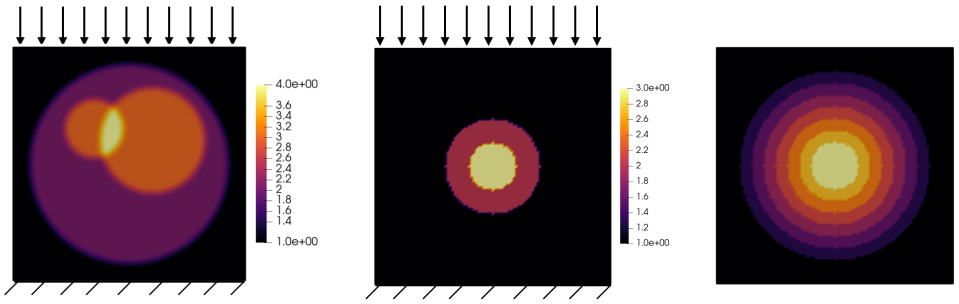

Figure 6. (a) Third model: three overlapping circular inclusions with the type of boundary condition used to generate the displacement field. (b) Fourth model: two overlapping inclusions used as the true parameter, along with the associated boundary condition. (c) Seven candidate circular inclusions used to reconstruct the parameter shown in (b).

To further investigate the noise sensitivity of the proposed method, we add noise of the form (7) to the displacement data and plot the relative reconstruction error in Figure 7 for both test cases. In both cases, the results show that even with a 30% noise level in the displacements, the relative error in the reconstructed shear modulus using the Type 1 virtual fields remains

around 20%. These results confirm once again that the proposed virtual fields are optimal in terms of robustness to noise.

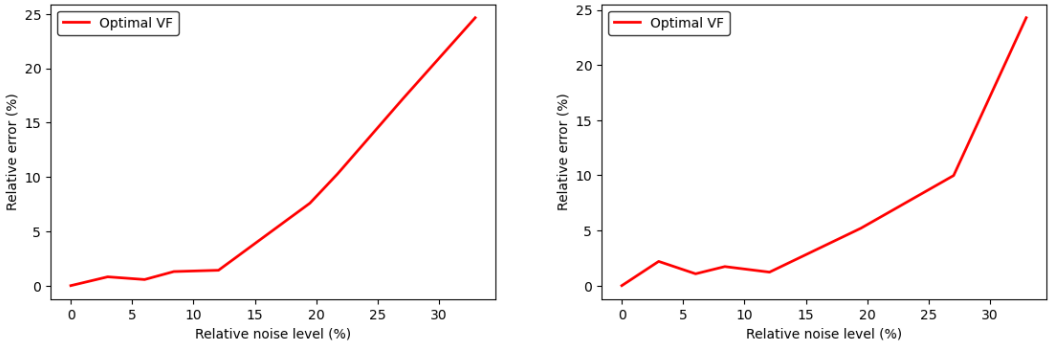

(a) **(b)**

Figure 7. Relative error for two different target shear modulus distributions under varying noise levels, using the proposed virtual fields: (a) third model, (b) fourth model.

4.2. *Homogeneous transversely isotropic compressible linear medium*

In this section, we consider two-dimensional transversely isotropic elasticity under the plane stress assumption. We focus on materials that are isotropic in one plane while exhibiting distinct mechanical properties along a perpendicular direction. Such behavior typically arises, for example, in fiber-reinforced composites, where fibers are aligned along a preferred orientation. Here, we assume that the axis of transverse isotropy is aligned with the x_1-direction. The displacement field $\mathbf{u}$ satisfies the following system of equations:

$$\begin{cases} \nabla \cdot \boldsymbol{\sigma} = \mathbf{0} & \text{in } \Omega, \\ \boldsymbol{\sigma} = \mathbb{C} : \boldsymbol{\varepsilon}(\mathbf{u}) & \text{in } \Omega, \\ \mathbf{u} = \mathbf{0} & \text{on } \Gamma_D, \\ \boldsymbol{\sigma} \cdot \boldsymbol{n} = \mathbf{t} & \text{on } \Gamma_N, \end{cases} \tag{56}$$

where $\boldsymbol{\sigma}$ denotes the Cauchy stress tensor, $\boldsymbol{\varepsilon}(\mathbf{u})$ the linearized strain tensor, and $\mathbb{C}$ the fourth-order elasticity tensor. In two dimensions, the constitutive law $\boldsymbol{\sigma} = \mathbb{C} : \boldsymbol{\varepsilon}$ is often expressed in Kelvin–Mandel notation, where both stresses and strains are represented as vectors, and the tensor $\mathbb{C}$ reduces to a symmetric positive-definite 3×3 matrix $[\mathbb{C}]$. The strain vector is written as

$$\boldsymbol{\varepsilon}(\mathbf{u}) = \begin{pmatrix} \varepsilon_{11} \\ \varepsilon_{22} \\ \sqrt{2}\varepsilon_{12} \end{pmatrix},$$

with $\varepsilon_{11} = \partial u_1/\partial x_1$, $\varepsilon_{22} = \partial u_2/\partial x_2$, and $\varepsilon_{12} = \frac{1}{2}(\partial u_1/\partial x_2 + \partial u_2/\partial x_1)$. The compliance matrix $[\mathbb{S}]$, which relates strain to stress via $\boldsymbol{\varepsilon} = [\mathbb{S}]\boldsymbol{\sigma}$, is given by

$$[\mathbb{S}] = \begin{pmatrix} \dfrac{1}{E_T} & -\dfrac{\nu_L}{E_L} & 0 \\ -\dfrac{\nu_L}{E_L} & \dfrac{1}{E_L} & 0 \\ 0 & 0 & \dfrac{1}{2G_L} \end{pmatrix},$$

where E_L is the Young's modulus along the preferred (longitudinal) direction, E_T is the Young's modulus in the transverse direction, ν_L is the Poisson's ratio that describes transverse strain in response to longitudinal stress, and G_L is the in-plane shear modulus. Inverting the compliance matrix yields the elasticity matrix $[\mathbb{C}] = [\mathbb{S}]^{-1}$, which takes the form

$$[\mathbb{C}] = \begin{pmatrix} \dfrac{E_L E_T}{E_L - E_T \nu_L^2} & \dfrac{E_L E_T \nu_L}{E_L - E_T \nu_L^2} & 0 \\ \dfrac{E_L E_T \nu_L}{E_L - E_T \nu_L^2} & \dfrac{E_L^2}{E_L - E_T \nu_L^2} & 0 \\ 0 & 0 & 2G_L \end{pmatrix}.$$

Reconstruction of elastic parameters. We assume, for simplicity, that the material is homogeneous, and we aim to reconstruct the four elastic parameters: E_L, E_T, G_L, and ν_L. Denoting the entries of the elasticity matrix by C_{11}, C_{12}, C_{22}, and C_{33}, we have:

$$C_{11} = \frac{E_L E_T}{E_L - E_T \nu_L^2}, \quad C_{12} = \frac{E_L E_T \nu_L}{E_L - E_T \nu_L^2}, \quad C_{22} = \frac{E_L^2}{E_L - E_T \nu_L^2}, \quad C_{33} = 2G_L.$$

Under these notations, the principle of virtual work (1) takes the form:

$$C_{11} \int_\Omega \varepsilon_{11}\,\varepsilon_{11}(\mathbf{v})\,\mathrm{d}\Omega + C_{22} \int_\Omega \varepsilon_{22}\,\varepsilon_{22}(\mathbf{v})\,\mathrm{d}\Omega + C_{12} \int_\Omega (\varepsilon_{11}\,\varepsilon_{22}(\mathbf{v}) + \varepsilon_{22}\,\varepsilon_{11}(\mathbf{v}))\,\mathrm{d}\Omega + 2C_{33} \int_\Omega \varepsilon_{12}\,\varepsilon_{12}(\mathbf{v})\,\mathrm{d}\Omega = \int_{\Gamma_N} \mathbf{t}\cdot\mathbf{v}\,\mathrm{d}S,$$

where $\mathbf{v} \in \mathbf{V}_0$ denotes a kinematically admissible virtual displacement field, and $\varepsilon_{ij}(\mathbf{v})$ are the components of the corresponding virtual strain tensor.

To identify the four unknown parameters, we follow the approach described in Section 2.4.2. By selecting four appropriately virtual displacement fields $\mathbf{v}_1$, $\mathbf{v}_2$, $\mathbf{v}_3$, and $\mathbf{v}_4$, we derive a linear system that allows the recovery of the material coefficients C_{11}, C_{12}, C_{22}, and C_{33}, and consequently of the parameters E_L, E_T, ν_L, and G_L. It should be noted that, in this case, the loading traction $\mathbf{t}$ must be known.

The material parameters are obtained by solving the linear system $\boldsymbol{A}\cdot\boldsymbol{C} = \boldsymbol{\lambda}$, where:

$$\boldsymbol{A} = \begin{pmatrix} \displaystyle\int_\Omega \varepsilon_{11}\varepsilon_{11}(\mathbf{v}_1)\,\mathrm{d}\Omega & \displaystyle\int_\Omega \varepsilon_{22}\varepsilon_{22}(\mathbf{v}_1)\,\mathrm{d}\Omega & \displaystyle\int_\Omega (\varepsilon_{11}\varepsilon_{22}(\mathbf{v}_1) + \varepsilon_{22}\varepsilon_{11}(\mathbf{v}_1))\,\mathrm{d}\Omega & 2\displaystyle\int_\Omega \varepsilon_{12}\varepsilon_{12}(\mathbf{v}_1)\,\mathrm{d}\Omega \\ \displaystyle\int_\Omega \varepsilon_{11}\varepsilon_{11}(\mathbf{v}_2)\,\mathrm{d}\Omega & \displaystyle\int_\Omega \varepsilon_{22}\varepsilon_{22}(\mathbf{v}_2)\,\mathrm{d}\Omega & \displaystyle\int_\Omega (\varepsilon_{11}\varepsilon_{22}(\mathbf{v}_2) + \varepsilon_{22}\varepsilon_{11}(\mathbf{v}_2))\,\mathrm{d}\Omega & 2\displaystyle\int_\Omega \varepsilon_{12}\varepsilon_{12}(\mathbf{v}_2)\,\mathrm{d}\Omega \\ \displaystyle\int_\Omega \varepsilon_{11}\varepsilon_{11}(\mathbf{v}_3)\,\mathrm{d}\Omega & \displaystyle\int_\Omega \varepsilon_{22}\varepsilon_{22}(\mathbf{v}_3)\,\mathrm{d}\Omega & \displaystyle\int_\Omega (\varepsilon_{11}\varepsilon_{22}(\mathbf{v}_3) + \varepsilon_{22}\varepsilon_{11}(\mathbf{v}_3))\,\mathrm{d}\Omega & 2\displaystyle\int_\Omega \varepsilon_{12}\varepsilon_{12}(\mathbf{v}_3)\,\mathrm{d}\Omega \\ \displaystyle\int_\Omega \varepsilon_{11}\varepsilon_{11}(\mathbf{v}_4)\,\mathrm{d}\Omega & \displaystyle\int_\Omega \varepsilon_{22}\varepsilon_{22}(\mathbf{v}_4)\,\mathrm{d}\Omega & \displaystyle\int_\Omega (\varepsilon_{11}\varepsilon_{22}(\mathbf{v}_4) + \varepsilon_{22}\varepsilon_{11}(\mathbf{v}_4))\,\mathrm{d}\Omega & 2\displaystyle\int_\Omega \varepsilon_{12}\varepsilon_{12}(\mathbf{v}_4)\,\mathrm{d}\Omega \end{pmatrix},$$

$$\boldsymbol{C} = \begin{pmatrix} C_{11} \\ C_{22} \\ C_{12} \\ C_{33} \end{pmatrix}, \qquad \boldsymbol{\lambda} = \begin{pmatrix} \displaystyle\int_{\Gamma_N} \mathbf{t}\cdot\mathbf{v}_1\,\mathrm{d}\Gamma \\ \displaystyle\int_{\Gamma_N} \mathbf{t}\cdot\mathbf{v}_2\,\mathrm{d}\Gamma \\ \displaystyle\int_{\Gamma_N} \mathbf{t}\cdot\mathbf{v}_3\,\mathrm{d}\Gamma \\ \displaystyle\int_{\Gamma_N} \mathbf{t}\cdot\mathbf{v}_4\,\mathrm{d}S \end{pmatrix}.$$

Once the components C_{11}, C_{22}, C_{12}, and C_{33} are identified, the material parameters E_L, E_T, ν_L, and G_L are computed using the following relations:

$$E_L = \frac{C_{11}C_{22} - C_{12}^2}{C_{11}}, \qquad E_T = \frac{C_{11}C_{22} - C_{12}^2}{C_{22}}, \qquad \nu_L = \frac{C_{12}}{C_{11}}, \qquad G_L = \frac{C_{33}}{2}.$$

Stability estimate. Let $\mathbf{u}^\delta$ denote the noisy displacement measurements and $\mathbf{u}^0$ the noise-free displacement field, which is the solution to (56) associated with the true elastic coefficients C_{11}^0, C_{22}^0, C_{12}^0, and C_{33}^0. We denote by C_{11}^δ, C_{22}^δ, C_{12}^δ, and C_{33}^δ their respective reconstructions obtained from $\mathbf{u}^\delta$.

Let C_a denote the continuity constant satisfying

$$\left| C_{11}^0 \int_\Omega \varepsilon_{11}\,\varepsilon_{11}(\mathbf{v})\,\mathrm{d}\Omega + C_{22}^0 \int_\Omega \varepsilon_{22}\,\varepsilon_{22}(\mathbf{v})\,\mathrm{d}\Omega \right.$$
$$\left. + C_{12}^0 \int_\Omega \big(\varepsilon_{11}\,\varepsilon_{22}(\mathbf{v}) + \varepsilon_{22}\,\varepsilon_{11}(\mathbf{v})\big)\,\mathrm{d}\Omega + 2C_{33}^0 \int_\Omega \varepsilon_{12}\,\varepsilon_{12}(\mathbf{v})\,\mathrm{d}\Omega \right| \le C_a\,\|\mathbf{u}\|_{\mathbf{V}}\,\|\mathbf{v}\|_{\mathbf{V}}.$$

As established in Section 2.4.3, the following stability estimates hold:

$$|C_{11}^\delta - C_{11}^0| \le \frac{C_a}{\left|\int_\Omega \varepsilon_{11}^\delta\,\varepsilon_{11}(\mathbf{v}_1^\delta)\,\mathrm{d}\Omega\right|}\,\|\mathbf{u}^\delta - \mathbf{u}^0\|_{H^1(\Omega)},$$
$$|C_{22}^\delta - C_{22}^0| \le \frac{C_a}{\left|\int_\Omega \varepsilon_{22}^\delta\,\varepsilon_{22}(\mathbf{v}_2^\delta)\,\mathrm{d}\Omega\right|}\,\|\mathbf{u}^\delta - \mathbf{u}^0\|_{H^1(\Omega)},$$
$$|C_{12}^\delta - C_{12}^0| \le \frac{C_a}{\left|\int_\Omega \big(\varepsilon_{11}^\delta\,\varepsilon_{22}(\mathbf{v}_3^\delta) + \varepsilon_{22}^\delta\,\varepsilon_{11}(\mathbf{v}_3^\delta)\big)\,\mathrm{d}\Omega\right|}\,\|\mathbf{u}^\delta - \mathbf{u}^0\|_{H^1(\Omega)},$$
$$|C_{33}^\delta - C_{33}^0| \le \frac{C_a}{\left|\int_\Omega 2\varepsilon_{12}^\delta\,\varepsilon_{12}(\mathbf{v}_4^\delta)\,\mathrm{d}\Omega\right|}\,\|\mathbf{u}^\delta - \mathbf{u}^0\|_{H^1(\Omega)}.$$

Numerical implementation and results. In what follows, we present numerical results to assess the effectiveness of the proposed approach for reconstructing homogeneous material properties in transversely isotropic elasticity, where the parameter vector is defined as

$$\mathbf{P} = (E_L, E_T, \nu_L, G_L).$$

Table 1. Reference material properties of a compressible transversely isotropic medium.

Material property	Symbol	Reference value	Unit
Longitudinal Young's modulus	E_L	10.5	MPa
Transverse Young's modulus	E_T	6.5	MPa
Poisson's ratio	ν_L	0.45	–
In-plane shear modulus	G_L	2.5	MPa

We consider a two-dimensional domain $\Omega = [0,1]^2$ and two distinct loading scenarios, in order to investigate how the internal displacement field measurements — and consequently the entries of the matrix $\boldsymbol{A}$ — influence the reconstruction stability.

The simulated displacement field $\mathbf{u}(\mathbf{P})$ is obtained by solving system (56), with $\mathbb{C} = \mathbb{C}(\mathbf{P})$, using the finite element method with a mesh size of $h = 1/50$. In both scenarios, the boundary Γ_D denotes the bottom edge of the domain Ω, while Γ_N represents the remaining part of the boundary. In the first scenario (Figure 8(a)), the Neumann boundary condition is prescribed as:

$$\mathbf{t} = \begin{cases} (1,-1) & \text{on } y = 1, \\ (0,0) & \text{elsewhere on } \Gamma_N. \end{cases}$$

In the second scenario (Figure 8(b)), the Neumann boundary condition is defined by:

$$\mathbf{t} = \begin{cases} (1,-1) & \text{on } x = 0, \\ (0,0) & \text{elsewhere on } \Gamma_N. \end{cases}$$

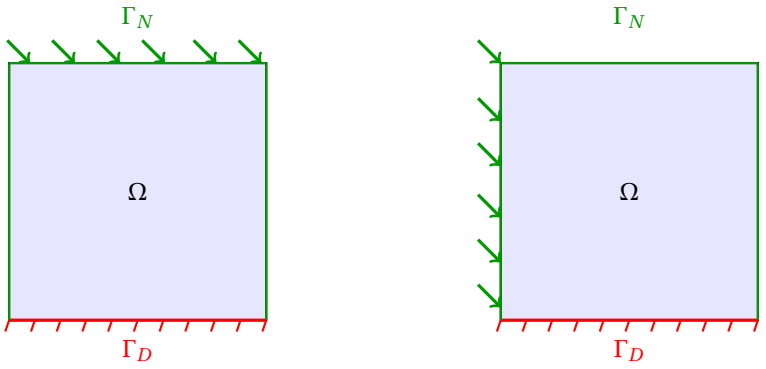

Figure 8. Geometry of the 2D linear elasticity problem (domain size 1.7 × 1.7).

To simulate experimental measurement uncertainty, we introduce spatially correlated multiplicative noise:

$$\mathbf{u}^\delta = \mathbf{u}(1+\chi_\delta), \quad \text{where} \quad \chi_\delta(x,y) = \delta(x^2+y^2) \tag{57}$$

where δ controls the noise amplitude.

We evaluate the reconstruction accuracy through the relative errors in the elasticity tensor coefficients:

$$\mathscr{E}_{C_{11}} = \frac{|C^\delta_{11} - C^0_{11}|}{|C^0_{11}|}, \qquad \mathscr{E}_{C_{22}} = \frac{|C^\delta_{22} - C^0_{22}|}{|C^0_{22}|}, \tag{58}$$

$$\mathscr{E}_{C_{12}} = \frac{|C^\delta_{12} - C^0_{12}|}{|C^0_{12}|}, \qquad \mathscr{E}_{C_{33}} = \frac{|C^\delta_{33} - C^0_{33}|}{|C^0_{33}|}. \tag{59}$$

The relative noise level is quantified in the H^1-norm as:

$$\text{Relative noise level} = \frac{\|\mathbf{u}-\mathbf{u}^\delta\|_{H^1(\Omega)}}{\|\mathbf{u}\|_{H^1(\Omega)}} \times 100\%,$$

The relative errors in the reconstructed elasticity coefficients are plotted as functions of the noise level, for both loading scenarios. The results are shown in Figure 9.

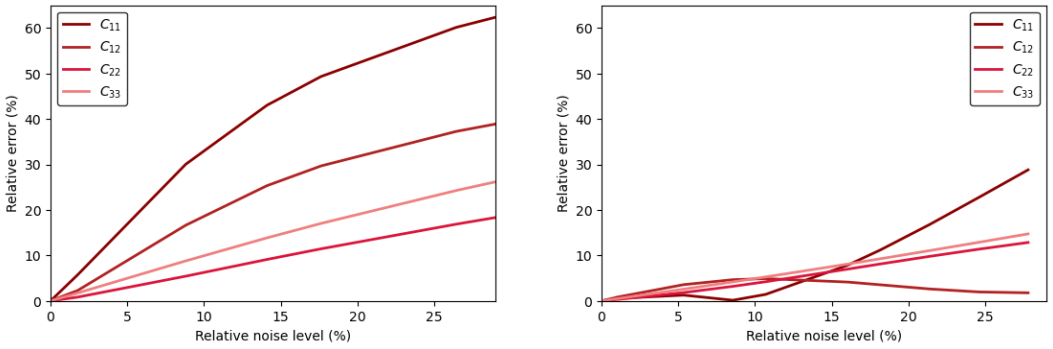

Figure 9. Relative errors in the components of the elasticity tensor as a function of noise level: (a) first loading scenario, (b) second loading scenario.

Discussion. By analyzing the results presented in Figure 9, we highlight the crucial role played by the structure of the displacement field in the stability of the reconstruction. In both scenarios, in the absence of noise, the reconstruction of all elasticity coefficients is highly accurate, with negligible relative errors.

In the first scenario, however, the reconstruction of C_{22} and C_{33} remains relatively stable, and the reconstruction error is well controlled (even with 25% noise, the reconstruction error is around 20%). In contrast, for the two coefficients C_{11} and C_{12}, the reconstruction is significantly less stable. This reflects the influence of the diagonal terms of the matrix $\boldsymbol{A}^{\delta}$ and, consequently, of the displacement field. In the second scenario, C_{12}, C_{22}, and C_{33} remain remarkably well reconstructed across all noise levels, whereas C_{11} is again the most sensitive coefficient, with an error exceeding 30 % for a noise level of about 30%. These results clearly demonstrate that the identifiability and robustness of each elasticity coefficient depend not only on the amount of noise but also on the displacement field induced by the loading and boundary conditions.

Furthermore, since we are interested in the parameters E_L, E_T, ν_L, and G_L, we define the relative errors for the effective elastic constants as follows:

$$\mathscr{E}_{E_L} = \frac{|E_L^{\delta} - E_L^0|}{|E_L^0|}, \qquad \mathscr{E}_{E_T} = \frac{|E_T^{\delta} - E_T^0|}{|E_T^0|}, \tag{60}$$

$$\mathscr{E}_{\nu_L} = \frac{|\nu_L^{\delta} - \nu_L^0|}{|\nu_L^0|}, \qquad \mathscr{E}_{G_L} = \frac{|G_L^{\delta} - G_L^0|}{|G_L^0|}. \tag{61}$$

Figure 10 shows the evolution of $\mathscr{E}_{E_L}$, $\mathscr{E}_{E_T}$, $\mathscr{E}_{\nu_L}$, and $\mathscr{E}_{G_L}$ as functions of the noise level for both loading configurations.

Although we do not derive a specific stability estimate for the effective parameters E_L, E_T, G_L, and ν_L, they inherently depend on the components of the elasticity tensor $\mathbb{C}$. Consequently, their sensitivity to noise reflects that of the underlying tensor. As shown in Figure 10, the first scenario exhibits significantly higher reconstruction errors across all parameters compared to the second scenario. This behavior is consistent with the overall improved stability observed in the second configuration.

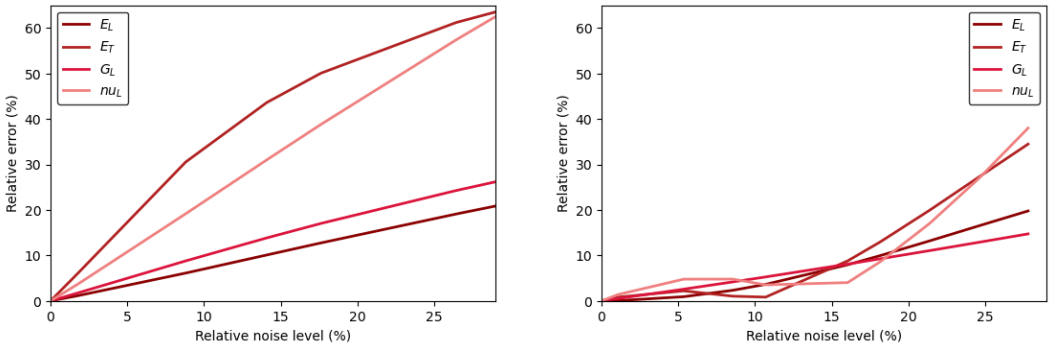

(a) **(b)**

Figure 10. Relative errors in the elastic parameters as a function of noise level: (a) first loading scenario, (b) second loading scenario.

5. Conclusion

To conclude, we have proposed a method for constructing virtual fields that are optimal in the sense of a precise stability estimate, in linear elasticity as well as in nonlinear elasticity,

provided that the constitutive law is linear with respect to the parameters to be identified. This ensures the stability of parameter reconstruction with respect to displacement measurement errors in the H^1-norm. The proposed method is rather general and applies to a wide range of situations. In particular, it is valid in any spatial dimension. It enables the reconstruction of homogeneous or heterogeneous material parameters when the structure is known a priori from a single displacement field using a direct and computationally efficient approach. Moreover, the method remains effective even in the presence of overlapping inclusions or when the material parameters are represented in a prescribed basis. No particular regularity or structure is required for the functions ϕ_i; they only need to be known and linearly independent. Finally, we note that in the present study we used deterministic noise for reproducibility. We do not address the important question of randomness in the noise and its impact on the solution. Such questions are interesting and could be explored in future work.

Declaration of interests

The authors do not work for, advise, own shares in, or receive funds from any organization that could benefit from this article, and have declared no affiliations other than their research organizations.

Underlying data

The underlying data for this article is available at https://doi.org/10.5281/zenodo.19629849 (see [46]).

References

[1] A. Tarantola, *Inverse problem theory and methods for model parameter estimation*, Society for Industrial and Applied Mathematics, 2005.

[2] M. Bonnet and A. Constantinescu, "Inverse problems in elasticity", *Inverse Probl.* **21** (2005), no. 2, R1.

[3] S. Avril, M. Bonnet, A.-S. Bretelle, et al., "Overview of identification methods of mechanical parameters based on full-field measurements", *Exp. Mech.* **48** (2008), no. 4, pp. 381–402.

[4] R. Chabiniok, P. Moireau, P.-F. Lesault, A. Rahmouni, J.-F. Deux and D. Chapelle, "Estimation of tissue contractility from cardiac cine-MRI using a biomechanical heart model", *Biomech. Model. Mechanobiol.* **11** (2012), no. 5, pp. 609–630.

[5] A. Gonsard, M. Genet and D. Drummond, "Digital twins for chronic lung diseases", *Eur. Respir. Rev.* **33** (2024), no. 174, article no. 240159 (15 pages).

[6] K. Hoyt, B. Castaneda, M. Zhang, et al., "Tissue elasticity properties as biomarkers for prostate cancer", *Cancer Biomarkers* **4** (2008), no. 4–5, pp. 213–225.

[7] R. Akhtar, M. J. Sherratt, J. K. Cruickshank and B. Derby, "Characterizing the elastic properties of tissues", *Mater. Today* **14** (2011), no. 3, pp. 96–105.

[8] D. Claire, F. Hild and S. Roux, "Identification of a damage law by using full-field displacement measurements", *Int. J. Damage Mech.* **16** (2007), no. 2, pp. 179–197.

[9] M. Grédiac and F. Hild (eds.), *Full-field measurements and identification in solid mechanics*, John Wiley & Sons, 2013.

[10] J.-L. Gennisson, T. Deffieux, E. Macé, G. Montaldo, M. Fink and M. Tanter, "Viscoelastic and anisotropic mechanical properties of in vivo muscle tissue assessed by supersonic shear imaging", *Ultrasound Med. Biol.* **36** (2010), no. 5, pp. 789–801.

[11] H. Rivaz, E. M. Boctor, M. A. Choti and G. D. Hager, "Real-time regularized ultrasound elastography", *IEEE Trans. Med. Imaging* **30** (2010), no. 4, pp. 928–945.

[12] R. Muthupillai, D. Lomas, P. Rossman, J. F. Greenleaf, A. Manduca and R. L. Ehman, "Magnetic resonance elastography by direct visualization of propagating acoustic strain waves", *Science* **269** (1995), no. 5232, pp. 1854–1857.

[13] A. K. Rutz, S. Ryf, S. Plein, P. Boesiger and S. Kozerke, "Accelerated whole-heart 3D CSPAMM for myocardial motion quantification", *Magn. Reson. Med.* **59** (2008), no. 4, pp. 755–763.

[14] J. M. Schmitt, "OCT elastography: imaging microscopic deformation and strain of tissue", *Opt. Express* **3** (1998), no. 6, pp. 199–211.

[15] F. Hild and S. Roux, "Digital image correlation: from displacement measurement to identification of elastic properties — A review", *Strain* **42** (2006), no. 2, pp. 69–80.

[16] K. M. Moerman, C. A. Holt, S. L. Evans and C. K. Simms, "Digital image correlation and finite element modelling as a method to determine mechanical properties of human soft tissue in vivo", *J. Biomech.* **42** (2009), no. 8, pp. 1150–1153.

[17] M. Genet, "Finite strain formulation of the discrete equilibrium gap principle: application to mechanically consistent regularization for large motion tracking", *Comptes Rendus. Mécanique* **351** (2023), no. G2, pp. 429–458.

[18] K. T. Kavanagh and R. W. Clough, "Finite element applications in the characterization of elastic solids", *Int. J. Solids Struct.* **7** (1971), no. 1, pp. 11–23.

[19] E. Pagnacco, A.-S. Caro-Bretelle and P. Ienny, "Parameter identification from mechanical field measurements using finite element model updating strategies", in *Full-Field Measurements and Identification in Solid Mechanics* (M. Grédiac and F. Hild, eds.), Wiley Publishing, 2013, pp. 247–274.

[20] A. Peyraut and M. Genet, "Finite strain formulation of the discrete equilibrium gap principle: application to direct parameter estimation from large full-fields measurements", *Comptes Rendus. Mécanique* **353** (2025), no. G1, pp. 259–309.

[21] P. Ladeveze and D. Leguillon, "Error estimate procedure in the finite element method and applications", *SIAM J. Numer. Anal.* **20** (1983), no. 3, pp. 485–509.

[22] A. Constantinescu, "On the identification of elastic moduli from displacement-force boundary measurements", *Inverse Probl. Eng.* **1** (1995), no. 4, pp. 293–313.

[23] E. Florentin and G. Lubineau, "Using constitutive equation gap method for identification of elastic material parameters: technical insights and illustrations", *Int. J. Interact. Des. Manuf.* **5** (2011), no. 4, pp. 227–234.

[24] D. Claire, F. Hild and S. Roux, "A finite element formulation to identify damage fields: the equilibrium gap method", *Int. J. Numer. Methods Eng.* **61** (2004), no. 2, pp. 189–208.

[25] S. Andrieux and A. B. Abda, "The reciprocity gap: a general concept for flaws identification problems", *Mech. Res. Commun.* **20** (1993), no. 5, pp. 415–420.

[26] S. Andrieux, H. D. Bui and A. Constantinescu, "Reciprocity gap method", in *Full-Field Measurements and Identification in Solid Mechanics* (M. Grédiac and F. Hild, eds.), Wiley Publishing, 2013, pp. 368–378.

[27] G. Bal, C. Bellis, S. Imperiale and F. Monard, "Reconstruction of constitutive parameters in isotropic linear elasticity from noisy full-field measurements", *Inverse Probl.* **30** (2014), no. 12, article no. 125004 (22 pages).

[28] H. Ammari, E. Bretin, P. Millien and L. Seppecher, "A direct linear inversion for discontinuous elastic parameters recovery from internal displacement information only", *Numer. Math.* **147** (2021), no. 1, pp. 189–226.

[29] N. Chibli, M. Genet and S. Imperiale, "Stability analysis of a new curl-based full field reconstruction method in 2D isotropic nearly-incompressible elasticity", 2025. To appear in *Inverse Probl.*

[30] A. N. Tikhonov and V. Y. Arsenin, *Solutions of ill posed problems*, John Wiley & Sons, 1977.

[31] H. W. Engl and R. Ramlau, "Regularization of inverse problems", in *Encyclopedia of applied and computational mathematics*, Springer, 2015, pp. 1233–1241.

[32] S. Roux and F. Hild, "Digital image mechanical identification (DIMI)", *Exp. Mech.* **48** (2008), no. 4, pp. 495–508.

[33] M. Grédiac, "Principe des travaux virtuels et identification", *C. R. Acad. Sci., Sér. II* **309** (1989), no. 1, pp. 1–5.

[34] M. Grediac, F. Pierron, S. Avril and E. Toussaint, "The virtual fields method for extracting constitutive parameters from full-field measurements: a review", *Strain* **42** (2006), no. 4, pp. 233–253.

[35] F. Pierron and M. Grédiac, *The virtual fields method: extracting constitutive mechanical parameters from full-field deformation measurements*, Springer, 2012.

[36] E. Toussaint, M. Grédiac and F. Pierron, "The virtual fields method with piecewise virtual fields", *Int. J. Mech. Sci.* **48** (2006), no. 3, pp. 256–264.

[37] S. Avril, M. Grédiac and F. Pierron, "Sensitivity of the virtual fields method to noisy data", *Comput. Mech.* **34** (2004), no. 6, pp. 439–452.

[38] T. T. Nguyen, J. M. Huntley, I. A. Ashcroft, P. D. Ruiz and F. Pierron, "A Fourier-series-based virtual fields method for the identification of 2-D stiffness distributions", *Int. J. Numer. Methods Eng.* **98** (2014), no. 12, pp. 917–936.

[39] Y. Mei, J. Deng, X. Guo, S. Goenezen and S. Avril, "Introducing regularization into the virtual fields method (VFM) to identify nonhomogeneous elastic property distributions", *Comput. Mech.* **67** (2021), no. 6, pp. 1581–1599.

[40] J. Deng, X. Guo, Y. Mei and S. Avril, "FEniCS implementation of the Virtual Fields Method (VFM) for nonhomogeneous hyperelastic identification", *Adv. Eng. Softw.* **175** (2023), article no. 103343.

[41] S. Avril and F. Pierron, "General framework for the identification of constitutive parameters from full-field measurements in linear elasticity", *Int. J. Solids Struct.* **44** (2007), no. 14–15, pp. 4978–5002.

[42] A. Marek, F. M. Davis and F. Pierron, "Sensitivity-based virtual fields for the non-linear virtual fields method", *Comput. Mech.* **60** (2017), no. 3, pp. 409–431.

[43] Y. Mei, J. Liu, X. Guo, B. Zimmerman, T. D. Nguyen and S. Avril, "General finite-element framework of the virtual fields method in nonlinear elasticity", *J. Elasticity* **145** (2021), no. 1, pp. 265–294.

[44] A. G. Holzapfel, *Nonlinear solid mechanics II*, John Wiley & Sons, 2000.

[45] Y. Mei and S. Avril, "On improving the accuracy of nonhomogeneous shear modulus identification in incompressible elasticity using the virtual fields method", *Int. J. Solids Struct.* **178** (2019), pp. 136–144.

[46] N. Chibli, M. Genet and S. Imperiale, *Optimal virtual fields Paper Demos*, Zenodo, software, v1.0, 2026. Online at https://zenodo.org/records/19629849.